LABORATORI NAZIONALI DI FRASCATI

SIS – Pubblicazioni

LNF–94/027 (IR)
31 Maggio 1994

Authomatic Alignment System for a Michelson Interferometer

D. Babusci, H. Fang, G. Giordano, G. Matone, V. Sannibale
INFN – Laboratori Nazionali di Frascati, P.O. Box 13, I–00044 Frascati (Roma) Italy

PACS.: 07.60.Ly; 04.80.+z

1 Introduction

The optical elements of the Virgo interferometer undergo position and angle fluctuations that are mostly due to the thermal and seismic noise. In general these are low-frequency fluctuations ($\leq 10\ Hz$) that can be rapidly damped if one has a system that is capable to detect the deviations and to intervene in a closed-loop circuit with the appropriate time scale. Since any angular tilt causes a variation of the length of the cavity and this can simulate a GW-signal, the specifications required for the angular stability are determined by the sensitivity level one is aiming at for the detection of a GW-signal. These can turn out to be very severe and thus the sensitivities required in monitoring the error signals can become an issue.

Let us consider a pure TEM_{00} laser beam impinging upon a plano-concave Fabry-Perot cavity under the condition of a perfect alignment and matching: the cavity and laser propagation axis are perfectly lined up and the beam waist lies on the plane mirror $M_1(M_3)$ with the right size (w_0) (see fig.(1)). If the laser beam does not drift in angle and/or position, a beam/cavity misalignment can occur only under one of these two circumstances (see fig.(1)):

i) an angular tilt of the input mirror $M_1(M_3)$ that causes a rotation and translation of the optical axis;

ii) an angular tilt or lateral displacement of the exit mirror $M_2(M_4)$ that both cause a lateral displacement of the optical axis;

or any linear combination of the above. Notice that any lateral diplacement of the mirror $M_1(M_3)$ is totally ineffective. A variation in the position and/or size of the beam waist does not affect the alignment but generates only a beam/cavity mismatching.

Let us consider the two above mentioned cases under the simplifying assumption that both the angle and/or position off-set occur only in one direction. If $L(= 3000\ m)$ is the

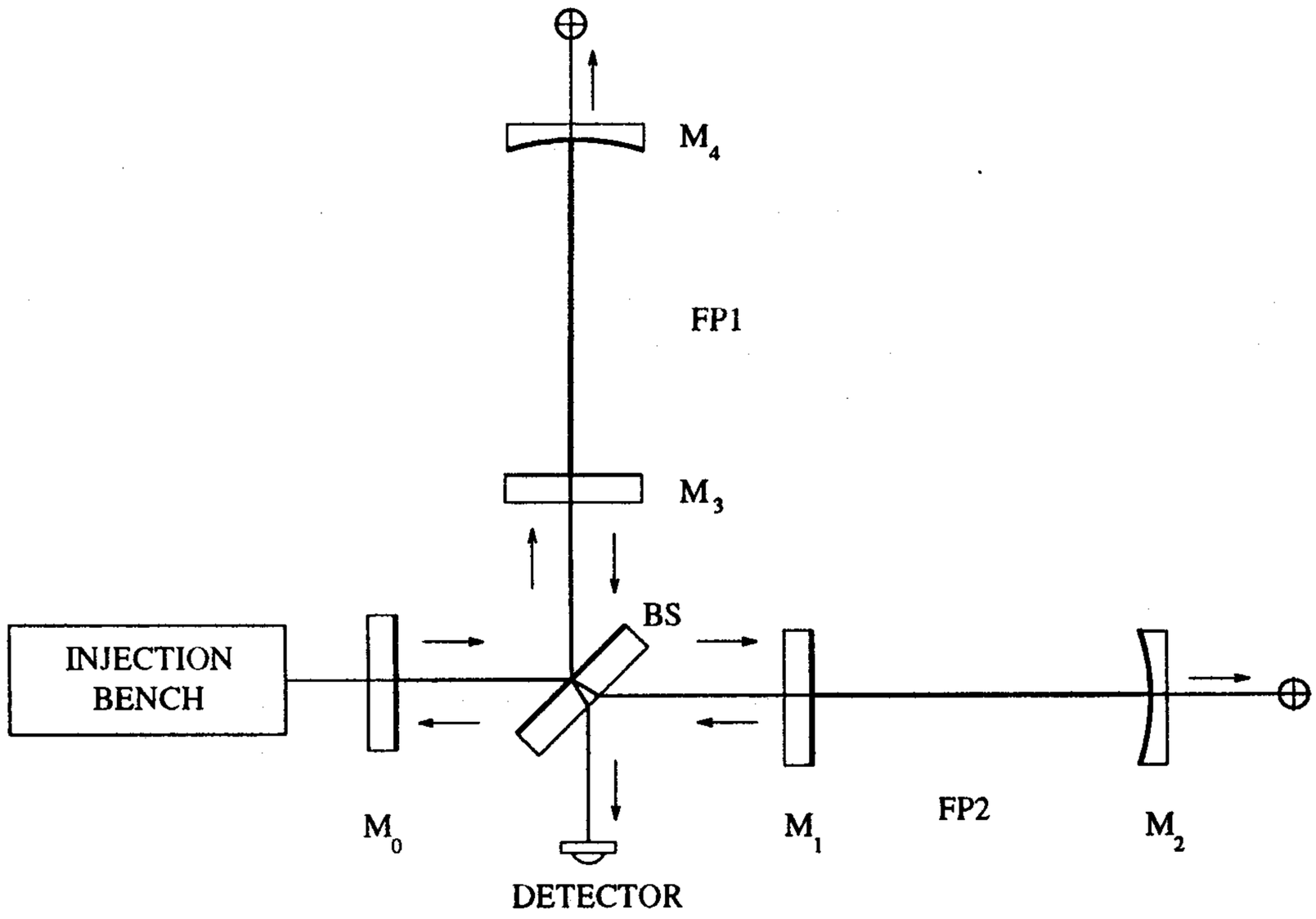

Figure 1: Michelson's interferometer scheme.

length of the cavity and $R(= 3450\ m)$ is the curvature radius of the mirror $M_2(M_4)$ the value of the "cavity parameter" $g = 1 - (L/R)$ is 0.13. With simple geometrical considerations it can be shown that

- an M_1-tilt $\Delta\theta$ generates
  1. a cavity axis rotation $\Delta\theta$
  2. a cavity axis displacement $\Delta x \simeq gR(\Delta\theta)$
  3. a cavity length variation

$$\frac{\Delta L}{L} = -\frac{1}{2}\left(\frac{g}{1-g}\right)(\Delta\theta)^2\ ; \tag{1}$$

- an M_2-tilt $(\Delta\theta)$ generates
  1. a cavity axis displacement $\Delta x = R(\Delta\theta)$
  2. a cavity length variation

$$\frac{\Delta L}{L} = \frac{1}{2}\left(\frac{1}{1-g}\right)(\Delta\theta)^2\ . \tag{2}$$

Notice that since $g = 0.13$, a tilt of the curved mirror M_2 (M_4) has an effect 10-times worse than the same tilt of the plane mirror $M_1(M_3)$. If for argument's sake, we assume a guess value of $\Delta L/L = 10^{-21}$, eqs.(1,2) state that the angular tilts of M_1 and M_2 must be controlled at better than $1.1 \cdot 10^{-10}\ rad$ and $4.2 \cdot 10^{-11} rad$, respectively.

The active alignment technique described in refs. [1, 2] has demonstrated sensitivities of $0.1\ nrad/\sqrt{Hz}$ to tilts and of $0.08\ nm/\sqrt{Hz}$ to lateral displacements for a single Fabry-Perot on a table-top configuration. Similar results have been obtained by using the "differential phase sensing technique" experimentally tested by the Glasgow group [3] on a single Fabry-Perot cavity. Both these results seem to be very promising. Here we consider a possible application of both these methods to the case of the Virgo interferometer.

2 The Anderson method

Let us consider a pure TEM_{00} laser beam entering a Fabry-Perot cavity with a tilting angle $\Delta\alpha$ with respect to the cavity axis. In the limit where this angle is much smaller than the far field divergence of the beam ($\lambda = 1.064\ \mu m$; $w_0 = 2\ cm$)

$$\alpha_0 = \frac{\lambda}{\pi w_0} = 1.69 \cdot 10^{-5}\ rad \tag{3}$$

it can be shown that the cavity sees the beam traveling along its axis as a linear superposition of the TEM_{00} distribution and the first off-axis mode TEM_{10}. Similarly, if the TEM_{00} beam enters the cavity with a lateral displacement Δx much smaller than the beam waist, the cavity sees again the incoming beam profile as a linear superposition of the TEM_{00} distribution and the first off-axis mode TEM_{10}.

The important difference between these two cases is that the rotations lead to a coupling into the TEM_{10} mode as the translations do, but with a 90° phase shift. This means that a misalignment causes a coupling to the lowest-order off axis mode with a phase that depends upon the type of misalignment. Therefore, the transverse field distribution seen by the cavity as a consequence of small walks off of the two terminal mirrors, can be always approximated by a linear combination of these two modes

$$E = C_0 U_0 + C U_1\ , \tag{4}$$

where E is the normalized input field, and U_0 and U_1 are the usual Hermite-Gaussian functions associated with the TEM_{00} and TEM_{10} modes. C_0 and C are the coupling coefficients and in general are complex numbers. In particular:

1. for a pure translation Δx: $\quad C = \Delta x / w_0$;
2. for a pure rotation $\Delta\alpha$: $\quad C = \imath\, \Delta\alpha / \alpha_0$;

and C_0 is always close to unity.

Furthermore, since M_1 can basically generate only rotations ($g \ll 1$) and M_2 only translations, the detection of a tilt or displacement type of error determines not only the extent of the drift but also the mirror that generated it. Therefore the basic idea of the method

is to find a way to detect the amplitude and phase of this induced TEM_{10} componenent. The logical place where to look at would be right behind the mirror M_2. But this presents an immediate problem. In a plano-concave cavity, the frequency difference between the fundamental mode and the first associated higher order mode, is given by:

$$\Delta\nu = \frac{c}{2\pi L}\arccos\left(\sqrt{g}\right) = 19.11\ kHz\ . \tag{5}$$

Consequently, if the cavity is tuned at one of the fundamental TEM_{00} longitudinal modes, which are frequency spaced of exactly $c/2L = 50\ KHz$, the TEM_{10} component introduced by the misalignment is necessarily off-resonance.

Following Appendix A, one has that in the Virgo case ($T_1^2 = 0.1$, $T_2^2 = 10^{-4}$) the ratio between the transmittivities on ($\cos 2kL = -1$) and off-resonance ($\cos 2kL = 1$) is given by

$$\frac{\mathcal{T}_{on}^2}{\mathcal{T}_{off}^2} = \left(\frac{1+R_1}{1-R_1}\right)^2 = 1444\,. \tag{6}$$

This means that very little of the power associated with the TEM_{10} is transmitted by the cavity. An elegant way out from this problem is offered by the optical heterodyne technique where phase modulation generates sidebands with the same frequency spacing that separates the first order mode from the fundamental TEM_{00} mode [2]. The field amplitude for a beam of phase modulated light at the optical frequency ω, has the form

$$E = E_0 e^{\imath\omega t}\Big\{J_0(m) + \sum_{l=1}^{l=\infty} J_l(m)[\,e^{\imath\Omega t} + (-)^l e^{-\imath\Omega t}\,]\Big\}\,, \tag{7}$$

where $\Omega = 2\pi\Delta\nu$ is the modulation frequency, E_0 is a constant real vector, and $J_l(m)$ is the Bessel function of order l and phase modulation index m. In this notation, the physical electric field is obtained by taking the real part of the complex quantities. For small values of the modulation index m only the first three in the expansion (7) can be retained and the expression of the electric field (4) reduces to :

$$E \simeq E_0\,(U_0 + CU_1)\,e^{\imath\omega t}\left\{J_0(m) + 2\imath J_1(m)\sin(\Omega t)\right\}\,. \tag{8}$$

By disregarding the non resonant terms in $(\omega - \Omega)$, this equation shows that the transmitted beam consists mostly of the fundamental mode at the carrier frequency with a small contribution from the TEM_{10} mode at the sideband frequency $(\omega + \Omega)$ [2]. The resulting transmitted intensity exhibits a spatially dependent component modulated at the beat frequency Ω as follows ($I_0 = \mid E_0 \mid^2$):

$$\begin{aligned} I = \mathcal{T}^2 \mid E \mid^2 = I_0\Big\{ & J_0^2\,U_0^2 + C^2\,J_1^2\,U_1^2 \\ & + 2J_0J_1U_0U_1\,[\mathcal{R}e(C)\cos\Omega t + \mathcal{I}m(C)\sin\Omega t\,]\Big\}\,. \end{aligned} \tag{9}$$

Since the Hermite-Gaussian functions are mutually orthogonal when integrated all over space, the detection of the entire transmitted beam by a single photodiode results in a DC-signal. The correspondent DC-photocurrent is obtained by integrating the first and leading

term of eq.(8) yielding

$$I_{dc} = \eta \frac{e\lambda}{hc} T^2 I_0 J_0^2(m) , \tag{10}$$

where η is the quantum efficiency (=0.8). On the contrary, a separate detection of each half of the transmitted beam, followed by electronic subtraction of the two photocurrents, yields a current signal given by

$$I_{diff} = 2\sqrt{\frac{2}{\pi}} I_{dc} \frac{J_1}{J_0} \left\{ \mathcal{R}e(C) \cos \Omega t + \mathcal{I}m(C) \sin \Omega t \right\} . \tag{11}$$

Eq.(11) shows that the intensity modulation that is in-phase with the modulation is proportional to the translational error and the quadrature signal is proportional to the angular alignment error. Thus, by selecting the proper demodulation phase, one can obtain both the error signals simultaneously and independently. With the same argument, a quadrant photodiode detector permits simultaneous detection of couplings to both vertical and horizontal off-axis modes.

3 Shot noise limitations

The result of the method, expressed by eqs.(10,11), says that the error signal is related to the measurement of the difference between two almost equal currents. Ultimately, this problem reduces to that of taking the difference between two almost equal numbers and, thus, the method finds its intrinsic limitation in the photon statistics. The *rms* shot noise current associated with eq.(10) is

$$I_{sn} = \sqrt{eI_{dc}} , \tag{12}$$

and the displacement and/or tilt that corresponds to a signal to noise ratio equal to one, turns out to be

$$| C | = \frac{1}{2J_1} \sqrt{\frac{\pi e}{2I_{dc}}} . \tag{13}$$

4 Coupling between the two FP-cavities

The case where one wants to apply this method to control simultaneusly the two arms of the Virgo interferometer presents a potential problem. Since the laser light bounces continuously between the two Fabry-Perot (FP_1 and FP_2), the information relative to a misalignment of one is inevitably transferred to the other one and viceversa. The extent of this coupling effect is anything but neglegible and can be seen in the following way.

Let us consider the frequency modulated laser beam that leaves the recycling mirror, is split by the beam splitter and impinges upon the front mirrors of the two FP's as shown in fig.(1). Let us suppose that initially the two cavities are perfectly aligned and, all of a sudden, independent misalignments occour in both FP_1 and FP_2. Two TEM_{10} components will immediately appear in both the transmitted and reflected beams from $FP_{1,2}$. These components will be recycled trough the whole interferometer and, after some transient time, an equilibrium condition will be reached. At this point, the two signals detected behind the two terminal mirrors will be a linear combination of the displacements $a_{1,2}$ and the angular tilts $\alpha_{1,2}$. This combination can be analytically calculated if the following simplifying hypothesis are assumed:

1. the recycling mirror and the beam splitter remain perfectly aligned;
2. the dephasing generated by a reflection from a FP-cavity is always $\mp 90^\circ$ depending if the wave-frequency is resonant or non-resonant in the cavity;
3. the frequency difference between the main carrier and the lateral sidebands is neglected in propagating the beam through the recycling cavity;
4. the component at the carrier frequency is assumed to estinguish on the output port (dark fringe condition).

Under these conditions, the complete calculation of the recycling process leads to the following expression for the powers P_1 transmitted behind the FP_1-terminal mirror:

$$\begin{aligned} P_1^{(L,R)} &= \frac{T_0^2 T_2^2 F}{4}\Big\{\Big(\frac{J_0}{1-\beta R_0}\Big)^2 + (A^2+B^2)\Big(\frac{J_1}{1+\beta R_0}\Big)^2 \\ &\pm \frac{4J_0J_1}{\sqrt{2\pi}(1-\beta^2R_0^2)}(A\cos\Omega t + B\sin\Omega t)\Big\} \\ &\qquad\qquad (+ = Left\ ,\ - = Right) \qquad (14) \\ P_1 &= P_1^{(L)} + P_1^{(R)} \end{aligned}$$

where $T_0^2(R_0^2)$ denote the transmittivity (reflectivity) of the recycling mirror, and

$$\begin{aligned} \beta &= \sqrt{1-T_2^2F} \\ A &= \frac{a_1 + a_2\beta R_0}{w_0(1-\beta R_0)} \qquad (15) \\ B &= \frac{\alpha_1}{\alpha_0} \end{aligned}$$

From eqs.(14,15) it's interesting to notice that the cross-talk between the two arms couples the two displacements only; neither angle/angle nor angle/displacement couplings are predicted. By assuming $R_0^2 = 0.95$ the extent of this coupling effect is ($\beta = 0.998$):

$$\beta R_0 = 0.97 \qquad (16)$$

which is very close to one and thus potentially dangerous for a good functioning of the feed-back system. By neglecting the term in J_1^2, the left/right asymmetry, which is free from systematic errors, is given by

$$A_s = \frac{Left - Right}{Left + Right} = \frac{8}{\sqrt{2\pi}} \frac{J_1}{J_0} \frac{1 - \beta R_0}{1 + \beta R_0} (A \cos \Omega t + B \sin \Omega t) \,. \tag{17}$$

With this equation we are now in the position to give a more realistic estimate of the minimum angle and lateral off-set that can be appreciated.

Let us suppose that the maximum power impinging upon the photodiode cannot exced $10\ mW$. According to eq.(10) and assuming $\eta = 0.8$, $J_0 = 1$, the corresponding total output current is $I_{max} = 6.85\ mA$. The minimum asymmetry that can be appreciated is:

$$A_s^{min} = \sqrt{\frac{e}{I_{max}}} = 4.8 \cdot 10^{-9} / \sqrt{Hz} \,. \tag{18}$$

Following eq.(15,17) we get:

$$\frac{\alpha_1^{min}}{\alpha_0} = \frac{\sqrt{2\pi}}{8} \frac{J_0}{J_1} \frac{1 + \beta R_0}{1 - \beta R_0} A_s^{min} = 9.9 \cdot 10^{-7} / \sqrt{Hz} \,, \tag{19}$$

and, assuming FP_2 aligned ($a_2 = 0$)

$$\frac{a_1^{min}}{w_0} = (1 - \beta R_0) \Big(\frac{\alpha_1^{min}}{\alpha_0} \Big) = 3.0 \cdot 10^{-8} / \sqrt{Hz} \,. \tag{20}$$

5 The Feed-Back System

Fig.(2) shows the basic conceptual scheme of the servo-loop mechanism that we have in mind.

For the time being, only tilts and displacements in one plane will be considered. The signals from each pair of photodiode detectors located behind the two M_2-mirrors are fed into a lock-in amplifier toghether with the reference frequency at $19.1\ kHz$ given by eq.(5). The two outputs are proportional to the in-phase and quadrature components associated with the lateral and angular displacements and constitute the error signals. For what we have been saying so far, these signals receive the extra contributions that are induced by the cross-talk between FP_1 and FP_2 and can be expressed in the following form ($h = \beta R_0$):

$$\begin{aligned} V_1^{(a)} &= k^{(a)} X_1^{(a)} \,, \quad & V_1^{(t)} &= k^{(t)} (X_1^{(t)} + h X_2^{(t)}) \\ V_2^{(a)} &= k^{(a)} X_2^{(a)} \,, \quad & V_2^{(t)} &= k^{(t)} (X_2^{(t)} + h X_1^{(t)}) \end{aligned} \tag{21}$$

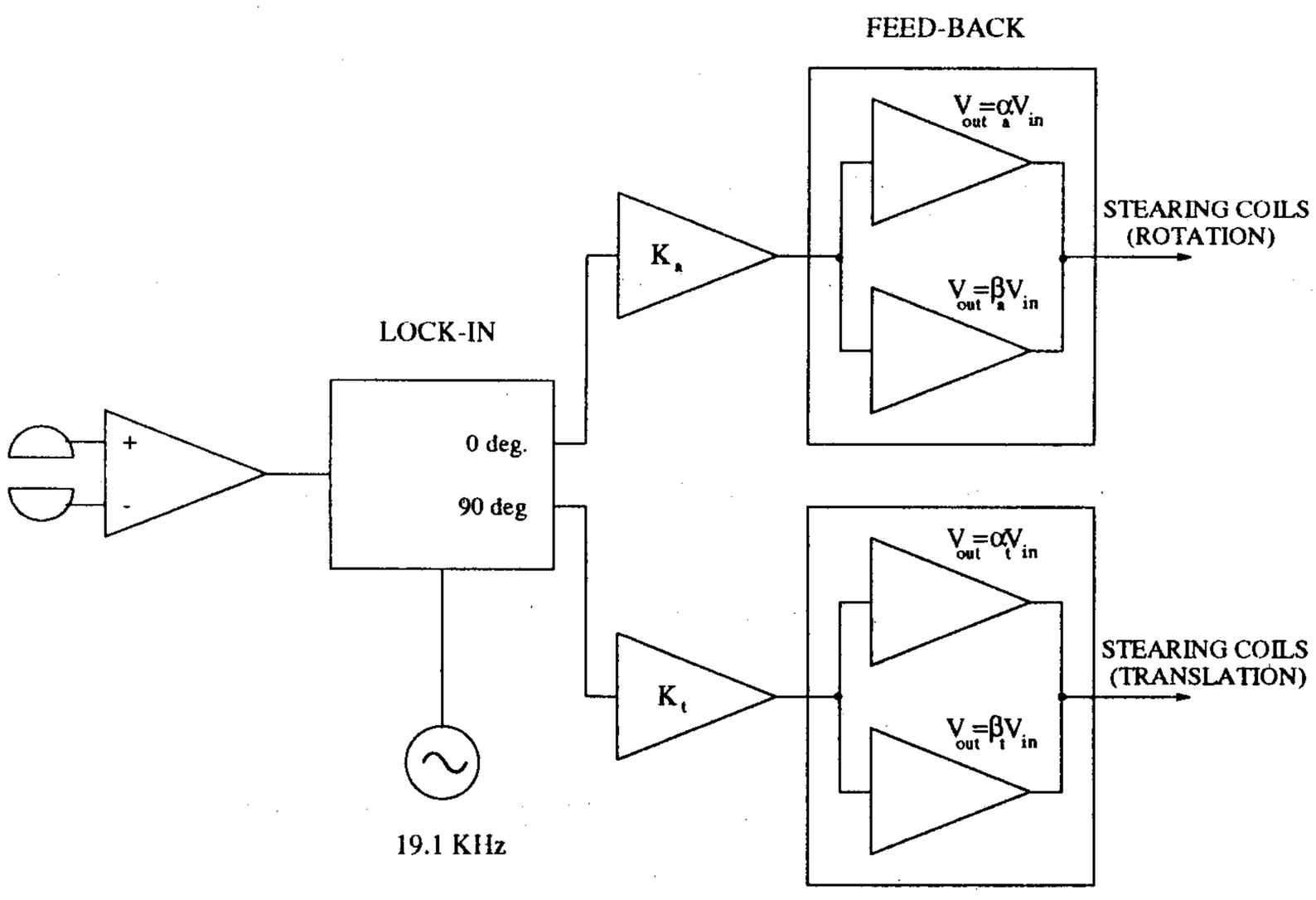

Figure 2: Conceptual scheme of the servo loop mechanism.

where we introduced a label to distinguish the angular (a) and the lateral (t) displacements. The parameters $k^{(a)}$ and $k^{(t)}$ are the amplification factors for tilts and translations, respectively.

Following a basic feed-back scheme, the voltage of eqs.(21) are first amplified and then plugged into linear filters. Each linear filters is programmed so as to generate a linear combination of these error signals and their first derivatives. For the time being the integrations will be ignored. These combinations are transformed into voltages and, by subsequent application to the steering coils, act on the mirrors and determine their accelerations if these mirrors can be considered as free suspended masses. Hence, as the final result of this elaboration, the motion of each degree of freedom will obey a second order differential equations. In practice, the mirrors are not free and the real action will be interfaced by the "marionetta mechanism" that introduces a transfer function between the correction signals and the final actuators on the mirrors. This will complicate the algorithm of the feed-back system but, at least in principle, shouldn't alter the generality of the present discussion. Therefore, if $\gamma^{(a,t)}$ and $\delta^{(a,t)}$ are the adjustable parameters of the linear combinations, with the definitions of eqs.(21), one has:

$$\begin{aligned} \ddot{X}_1^{(a)} &= \gamma^{(a)} k^{(a)} X_1^{(a)} + \delta^{(a)} k^{(a)} \dot{X}_1^{(a)} \\ \ddot{X}_2^{(a)} &= \gamma^{(a)} k^{(a)} X_2^{(a)} + \delta^{(a)} k^{(a)} \dot{X}_2^{(a)} \end{aligned} \tag{22}$$

and

$$\begin{aligned} \ddot{X}_1^{(t)} &= \gamma^{(t)}k^{(t)}(X_1^{(t)} + hX_2^{(t)}) + \delta^{(t)}k^{(t)}(\dot{X}_1^{(t)} + h\dot{X}_2^{(t)}) \\ \ddot{X}_2^{(t)} &= \gamma^{(t)}k^{(t)}(X_2^{(t)} + hX_1^{(t)}) + \delta^{(t)}k^{(t)}(\dot{X}_2^{(t)} + h\dot{X}_1^{(t)}) \end{aligned} \tag{23}$$

Eqs.(23) constitute a system of two linear and coupled differential equations with constant coefficients. With the positions:

$$r = X_1^{(t)} + X_2^{(t)}\,, \qquad q = X_2^{(t)} - X_1^{(t)} \tag{24}$$

it can be reduced to a system of two decoupled differential equations, for the variables r and q :

$$\begin{aligned} \ddot{r} - (1+h)k^{(t)}(\delta^{(t)}\dot{r} + \gamma^{(t)}r) = 0 \\ \ddot{q} - (1-h)k^{(t)}(\delta^{(t)}\dot{q} + \gamma^{(t)}q) = 0 \end{aligned} \tag{25}$$

An eye inspection of Eqs.(22,25) shows that the stability of the solutions requires

$$\begin{aligned} \gamma^{(l)},\ \delta^{(l)} &< 0 \qquad (l = a, t) \\ |\,h\,| &< 1 \end{aligned} \tag{26}$$

otherwise the feed-back system, as we have considered it, won't work. The coupling coefficient h introduces an asymmetry between the two eqs.(25) but, within the conditions of eqs.(26), the stability of the solutions is always guaranteed. However, it is evident that the stronger the coupling is and the higher the gain $k^{(t)}$ has to be.

6 Low-frequency noise suppression

Finally we have to consider the low-frequency damping effects. Eqs.(22,25) become stochastic equations if we consider a term on the right hand side representing the effect of additional random forces. These are due to all the noises that can disturb the suspended mirrors and have some determined spectral composition in frequency.

Let us consider the particular component at the frequency ω_0 and seek a particular solution of the inhomogeneous equation for q (or r)

$$\ddot{q} - (1-h)k^{(t)}(\delta^{(t)}\dot{q} + \gamma^{(t)}q) = Z_0\,\omega_0^2\,\sin\omega_0 t\,, \tag{27}$$

of the form

$$q = N\sin(\omega_0 t + \varphi)\,. \tag{28}$$

The result is very well known and yields:

$$N = \frac{Z_0\,\omega_0^2}{\sqrt{[\omega_0^2 + (1-h)k^{(t)}\gamma^{(t)}]^2 + [(1-h)k^{(t)}\delta^{(t)}\omega_0]^2}} \tag{29}$$

$$\varphi = \arctan\left\{ - \frac{(1-h)k^{(t)}\delta^{(t)}}{\omega_0^2 + (1-h)k^{(t)}\gamma^{(t)}}\,\omega_0 \right\}.$$

When the solution of the homogeneous eq.(27) has died off, only the term of eq.(28) survives. The amplitude q will follow the action of the external disturbing force with a different phase and a different amplitude. Moreover, eq.(29) shows that the feed-back mechanism has introduced a pole into the system with frequency and width given by:

$$\omega_{0R} = \sqrt{(h-1)k^{(t)}\gamma^{(t)}} \tag{30}$$

$$\Delta\omega_{0R} = \omega_{0R}^2\,\frac{\delta^{(t)}}{\gamma^{(t)}}\,.$$

If the gain is sufficiently high so that the pole is kept far above the region of interest ($10\ Hz$), the suppression factor s, defined as

$$s = \frac{N}{Z_0} = \frac{\omega_0^2}{\sqrt{\omega_0^2(\Delta\omega_{0R})^2 + (\omega_{0R}^2 - \omega_0^2)^2}}, \tag{31}$$

in the low frequency region becomes:

$$s = \left(\frac{\omega_0}{\omega_{0R}}\right)^2. \tag{32}$$

In conclusion, in spite of the presence of a strong coupling effect, the feed-back system will have a strong damping effect in the low-frequency region if the gain $(h-1)k^{(a)}\gamma^{(a)}$ can be made sufficiently high.

7 The Glasgow method: the differential phase sensing technique.

This alternative tecnique has been suggested by R.Drever at Caltech and experimentally demonstrated by H.Ward at the University of Glasgow [3]. It's basically an extension of the method that will be described for the longitudinal locking (Pound and Drever) and relies on using the light which is reflected from the input mirror. The beam is phase modulated

but the modulation frequency Ω is not to be equal to the frequency difference between fundamental and first transverse mode as it is in the Anderson method.

Let us suppose that the cavity is both laterally and angularly misaligned with respect to the incoming beam direction of the usual quantities a and α respectively. In the cavity frame the incoming beam is described by

$$E_{in} = E_0 e^{\imath\omega t}[U_0 + (a + \imath\alpha)U_1][J_0 + 2\imath J_1 \sin(\Omega t)] , \tag{33}$$

where the carrier frequency is resonant but the two sidebands ($\omega \pm \Omega$) are not. If the cavity is locked at resonance, the expression for the fully reflected beam in the main beam frame, follows from the second consideration of sec.4

$$E_{ref} = -\imath E_0 e^{\imath\omega t}[J_0(U_0 - 2aU_1) + 2\imath J_1(U_0 + 2\imath\alpha U_1)\sin(\Omega t)] . \tag{34}$$

The idea of the method is to let this beam evolve freely in space and to consider that an additional term intervenes in this process. This term is the phase difference between the real Gaussian beam and the ideal plane wave approximation given by

$$\phi_n(z) = (n+1)\phi(z) , \qquad \tan\phi(z) = \frac{\lambda z}{\pi w_0^2} = 8.2 \cdot 10^{-4} z . \tag{35}$$

The index n refers to the n-th order mode and z is the propagation coordinate whose origin, $z = 0$, is at the location of the beam waist. This means that different modes evolve differently and the two components U_0 and U_1 acquire the phase difference $\phi(z)$:

$$\begin{aligned} E_{ref} = -\imath E_0 e^{\imath\omega t} \Big\{ & [J_0(U_0 - 2aU_1\cos\phi) - 4\alpha J_1 \cos\phi \sin(\Omega t)] \\ & - 2\imath\,[aJ_0U_1\sin\phi + J_1(U_0 + 2\alpha U_1 \sin\phi)\sin(\Omega t)]\Big\} . \end{aligned} \tag{36}$$

The intensity associated with this field depends upon the position where the detector is located. If the current difference between the two halves of a photodetector is taken at a given z-position, and the signal is demodulated at the frequency Ω, the dominant component that will be detected is given by:

$$I_{diff} \propto -8J_0J_1U_0U_1(a\sin\phi + \alpha\cos\phi)\sin(\Omega t) . \tag{37}$$

The beam has a waist on M_1 and thus $\sin\phi = 0$ in eq.(37). Therefore, in the region right after the reflection the method is sensitive only to tilts. However, if the beam is let to evolve the $\sin\phi$ term builds up with distance and an equal sensitivity to angles and displacements is reached when $\phi = \pi/4$ or, in the Virgo case, for $z = 1219.5\ m$. The same distance, for the Frascati interferometer would be 298.2 cm. In both cases these values can be considerably shortened with the introduction of an appropriate focusing lens. This has been discussed in detail in ref.[3].

At present we don't have any data on this method for our top bench interferometer.

8 The Frascati table-top interferometer

8.1 Generalities

As it has been mentioned above, the Anderson method has never been used to control the alignment of a Michelson interferometer with recycling and Fabry-Perot in the arms. The only experimental demonstration of power recycling in a such a system has been reported in [4, 5] where no informations about automatic alignment systems are given. To illuminate the practical difficulties one can encounter with a completely automatized system, we decided to construct a rigid prototype Michelson interferometer with commercial mounts on a small optical table. The lay-out is shown in fig.(3).

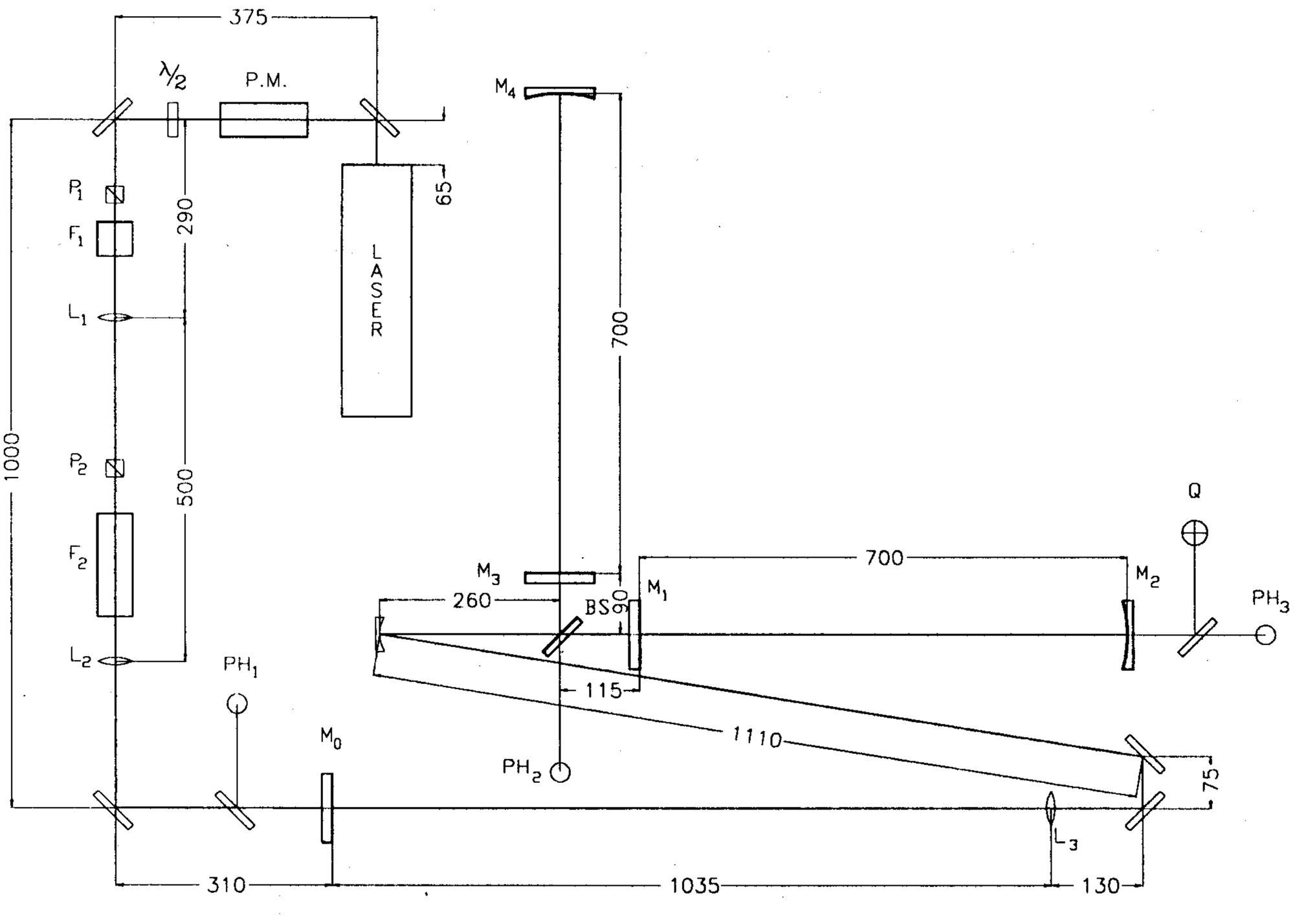

Figure 3: Frascati table top interferometer.

The laser is a small He-Ne (Newport-1 mW) and the two Fabry-Perot are plane-concave cavities. In the following table we summarized the main characteristics of the mirrors

Mirror	Label	Transmittivity	Curvature radius
recycling	M_0	$(1 \div 10)\%$	∞
input	M_1, M_3	$(1 \div 10)\%$	∞
output	M_2, M_4	$(0.02 \div 1)\%$	$10\ m$
beam splitter	BS	50%	∞

All the mirrors are mounted on Burleigh-(piezo mounting). The single Fabry-Perot cavity is $1\ m$ long and the separation between two longitudinal modes is $150\ MHz$. The transverse-longitudinal separation is $15\ MHz$. The line-width profile measured in transmission behind the terminal mirror is reported in fig.(4).

From the measured value of the width of the resonance

$$\frac{c/2L}{\Delta\nu} = \mathcal{F}(finesse) = \frac{\pi\sqrt{R_1 R_2}}{1 - R_1 R_2} = 111.1 \tag{38}$$

one has $R_1 R_2 = 0.974$ consistent with the values experimentally used $R_2 = 0.995$ and $R_1 = 0.975$.

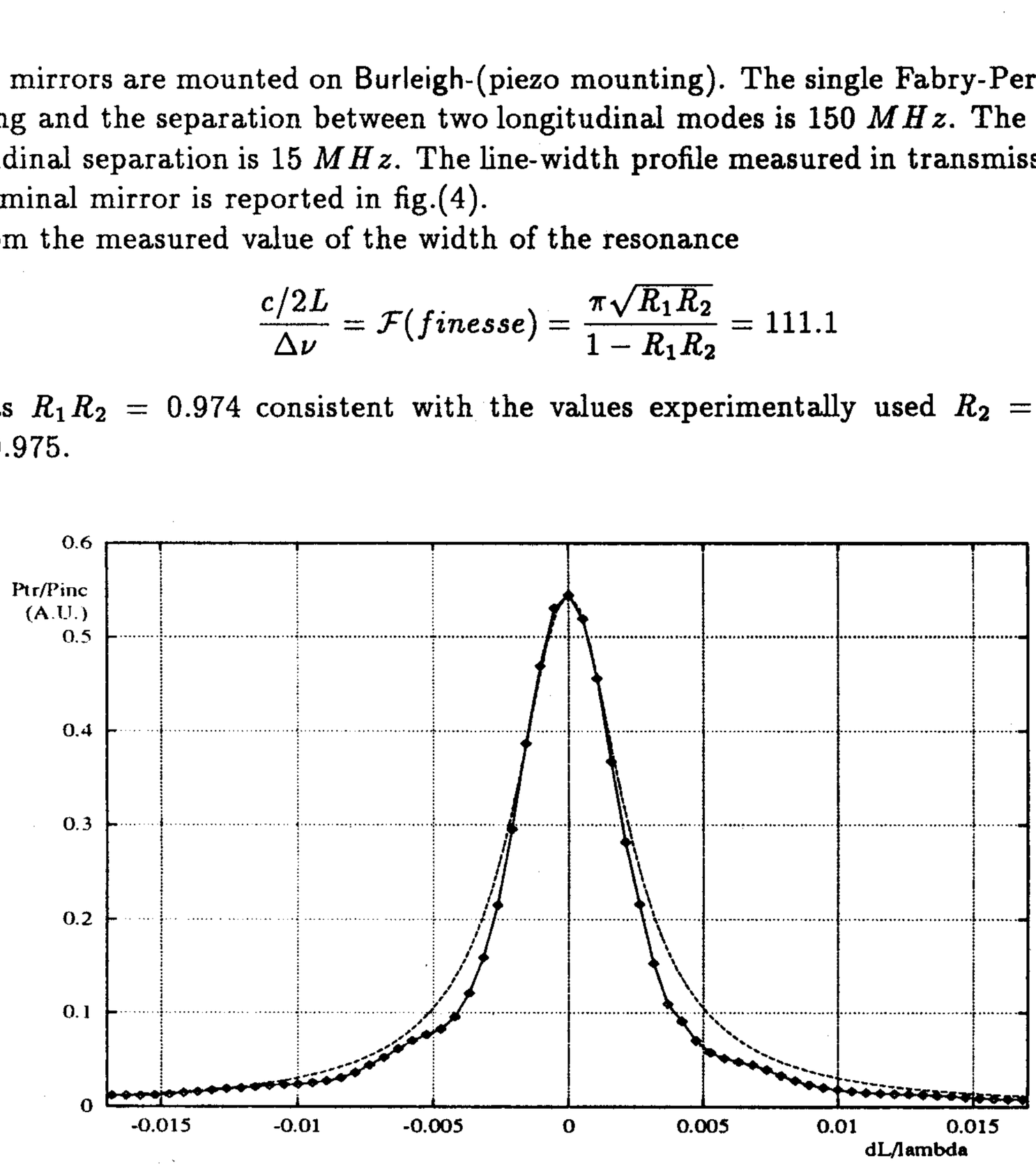

Figure 4: Line-width profile.

8.2 The Pound-Drever method

The single Fabry-Perot has been longitudinally locked using the Pound-Drever method technique [6]. The basic mechanism of this method can be summarized as follows.

Let's suppose to have a phase-modulated beam at the frequency (Ω) impinging upon the cavity and to look at the beam reflected back from the input mirror cavity $M_1(M_3)$. The expressions for the incident and reflected amplitudes are:

$$\begin{aligned} E_{inc} &= E_0\, e^{\imath\omega t}\Big\{J_0 + J_1\, e^{\imath\Omega t} - J_1\, e^{-\imath\Omega t}\Big\} \\ E_{ref} &= e^{\imath(\omega t+\phi_0)}\Big\{A_0 + A_+ e^{\imath(\Omega t+\phi_+ -\phi_0)} + A_- e^{-\imath(\Omega t+\phi_0-\phi_-)}\Big\} \end{aligned} \tag{39}$$

where ω is the beam frequency and the real quantities A_i $(i = 0, +, -)$ are the reflectivity functions of the Fabry-Perot. The corresponding expression for the reflected power is:

$$\begin{aligned} |\, E_{ref}\,|^2 = {} & |\, A_0\,|^2 + |\, A_+\,|^2 + |\, A_-\,|^2 \\ & + 2A_0A_+ \cos(\Omega t + \phi_+ - \phi_0) + 2A_0A_- \cos(\Omega t + \phi_0 - \phi_-) \\ & + 2A_+A_- \cos(2\Omega t + \phi_+ - \phi_-) \end{aligned} \tag{40}$$

which shows a DC-level and two components modulated at frequency Ω and 2Ω. If the two sidebands are completely off-resonance and we reasonably assume $\phi_+ = \phi_- = \pi/2$, the term in Ω of eq.(40) symplifies into

$$(A_+ + A_-)\sin\phi_0 \cos\Omega t - (A_+ - A_-)\cos\phi_0 \sin\Omega t\ . \tag{41}$$

Exactly at the resonance, one has:

$$\phi_0 = -\frac{\pi}{2}\ , \qquad A_+ + A_- = 0 \tag{42}$$

and both the sine and cosine terms vanish. The behaviours of these components when the cavity length is scanned through the resonance are shown in fig.(5,6).

In particular, the sine term exhibits a fast slope through zero, which is linear over a region of the order of $5 \cdot 10^{-3}$ of a wavelength. Thus this component is a nice candidate for being the error signal necessary to generate the correction to be applied to the piezo mount hosting the terminal mirror.

8.3 The length stabilization

The piezo mount has a frequency response that relates the applied voltage to the motion effectively executed by the mirror. This means that for any sinusoidal perturbation at a given frequency ω one has:

$$x(\omega) = G(\omega)V_{in}(\omega)\ , \tag{43}$$

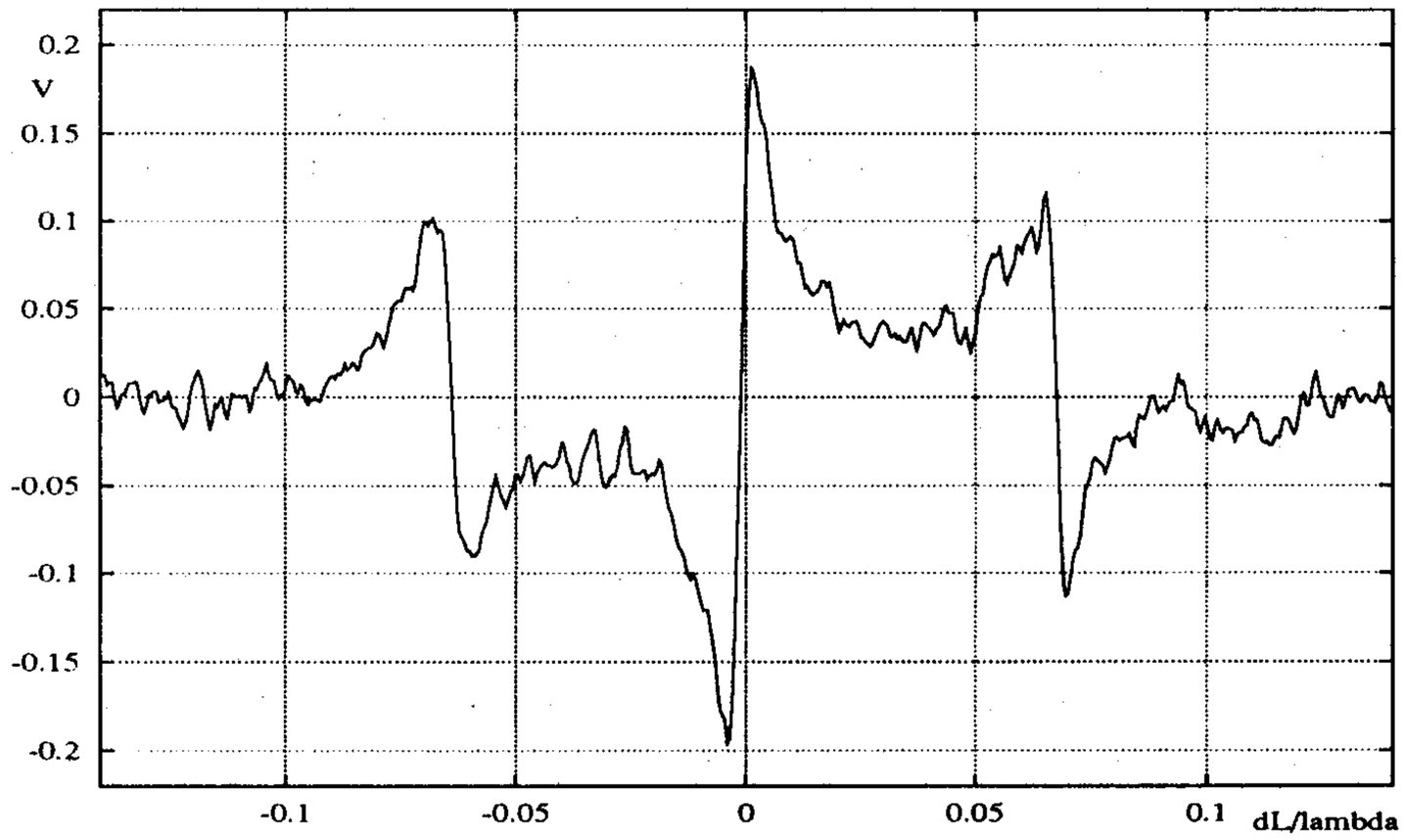

Figure 5: Pound-Drever method : $\sin \Omega t$ amplitude from eq.(40).

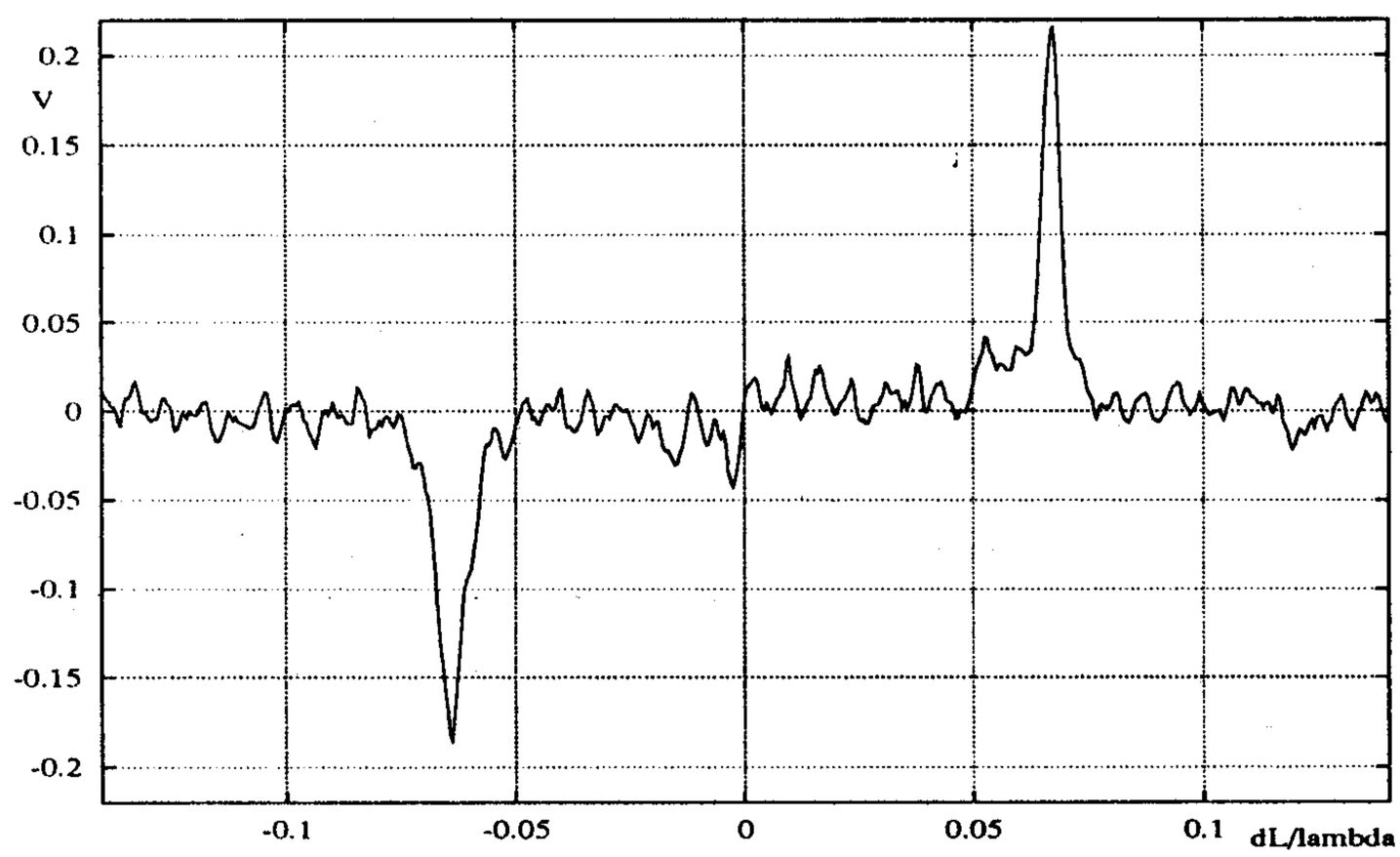

Figure 6: Pound-Drever method : $\cos \Omega t$ amplitude from eq.(40).

where $x(\omega)$ and $V_{in}(\omega)$ are the mirror position and piezo voltage amplitudes, respectively. The transfer function $G(\omega)$ is, in general, a complex function and, for a correct understanding of the feed-back system, has to be experimentally measured. A special set up has been arranged for this measurement. An acousto- optic modulator driven at 40 MHz generates a secondary component, which is up-shifted in frequency of the same amount and travels slightly tilted at an angle with respect to the main beam. This second component impinges upon the mirror holder which is set into oscillation by a voltage driving the piezo at a given amplitude and frequency. After being reflected by the mirror this component is summed with the main component that leaves the modulator unshifted. The signal that results from the beating between these two beams of different frequencies is demodulated at 40 MHz and yields the amplitude and phase of the actual movement of the mirror. This fully determines the transfer function of eq.(43). The experimental determinations of $G(\omega) = g(\omega)e^{\imath\psi(\omega)}$ are shown in fig.(7,8) in the frequency interval from zero to 800 Hz. The resonances visible in the region between 200 Hz and 500 Hz are of mechanical nature and have been efficiently damped by adding an extra load to the mount.

In the feed-back system that we used, the error signal described above, is first integrated, then amplified and finally, after some delay time τ, applied to the piezo. The mathematical translation of this procedure drives to a second order differential equation for the mirror position $x(t)$. If, similarly to what has been done in sec.6, a forcing term $Z_0 e^{\imath\omega_0 t}$ is supposed to act on the piezo mount, this equation can be written as:

$$\tau\ddot{x}(t) + \dot{x}(t) - kG(\omega_0)x(t) = \imath Z_0\,\omega_0 \exp(\imath\omega_0 t)\,, \tag{44}$$

where k is an overall amplification factor. The stability for the solution of the homogeneus equation (44) requires:

$$kg(\omega_0)\cos\psi(\omega_0) \;<\; 0 \tag{45}$$

and, at equilibrium, one has:

$$x(t) = x_0 \exp\left[\imath(\omega_0 t + \eta)\right]\,, \tag{46}$$

where $(g_0 = g(\omega_0); \psi_0 = \psi(\omega_0))$

$$x_0 = \frac{Z_0\omega_0}{\sqrt{k^2 g_0^2 + \omega_0^2(1+\tau^2\omega_0^2) + 2kg_0\omega_0(\tau\omega_0\cos\psi_0 - \sin\psi_0)}} \tag{47}$$

$$\eta = \arctan\left\{\frac{\tau\omega_0^2 + kg_0\cos\psi_0}{kg_0\sin\psi_0 - \omega_0}\right\}$$

In all practical cases, it's always

$$\tau\omega_0 \ll 1 \tag{48}$$

and, given our experimental conditions

$$k = 6.32\cdot 10^9\ V/cm\cdot s\,, \qquad g(\omega_0 = 0) = 2.0\cdot 10^{-7} cm/V\,, \tag{49}$$

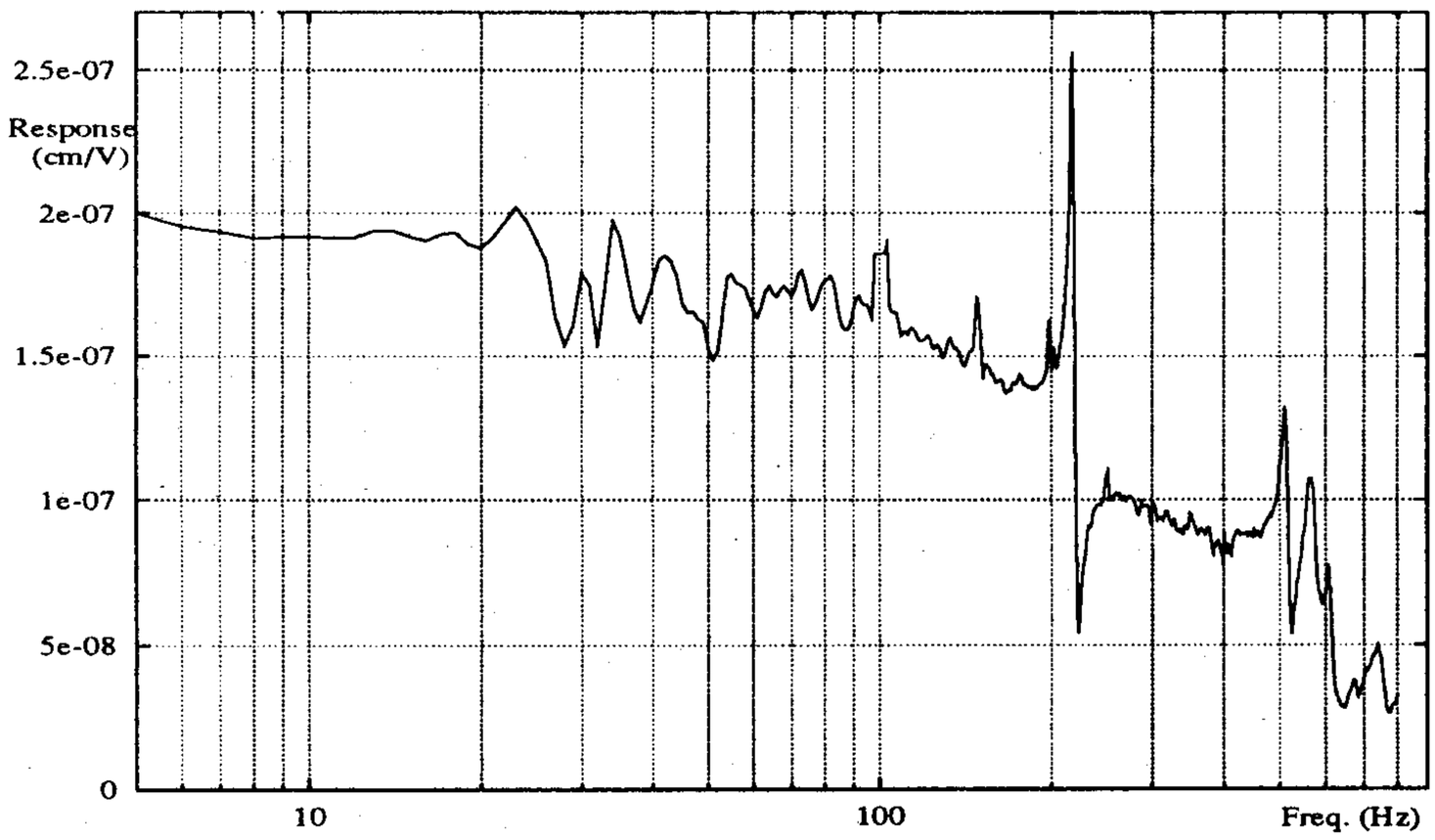

Figure 7: Transfer function : amplitude $g(\nu)$.

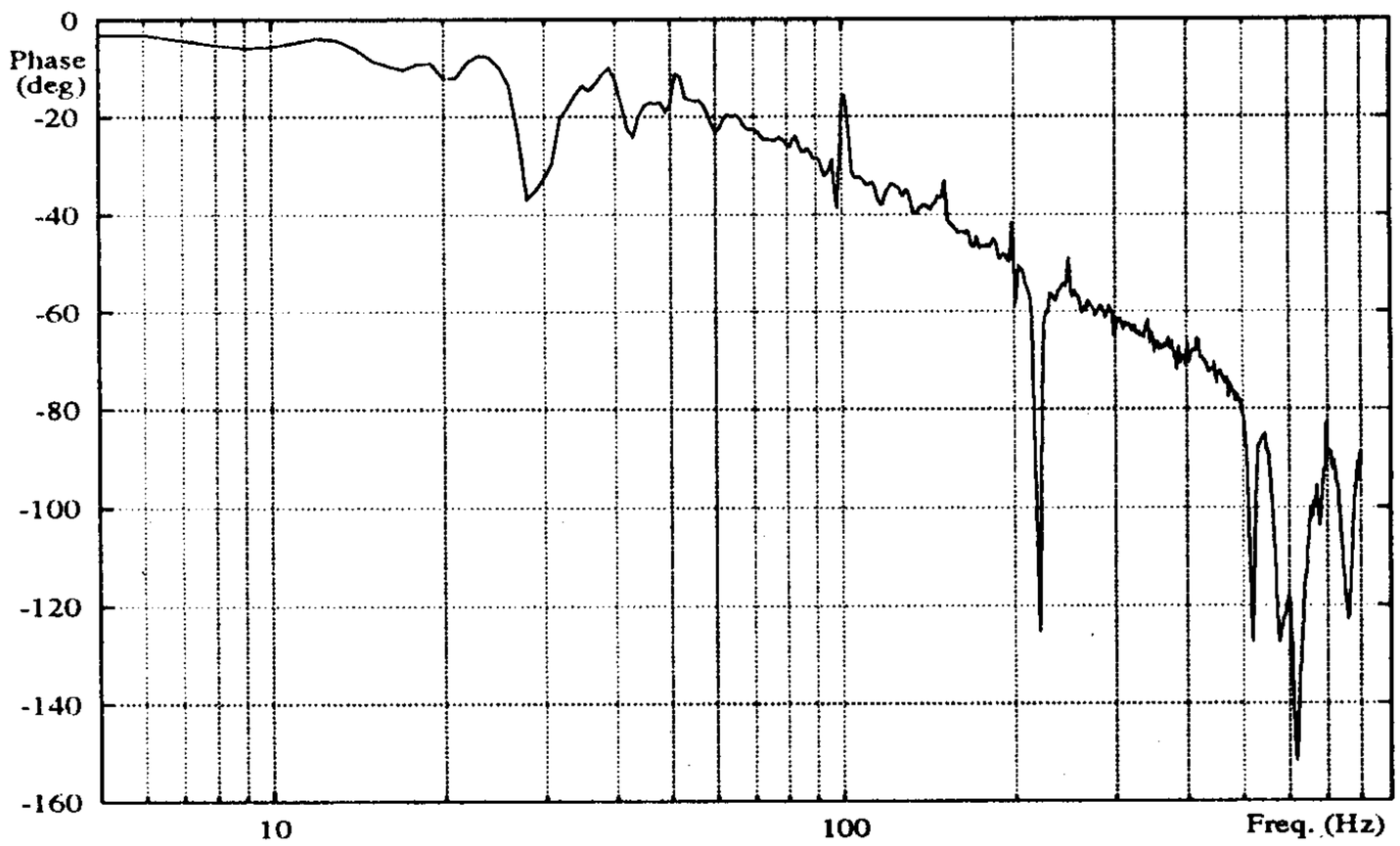

Figure 8: Transfer function : phase $\psi(\nu)$.

at low frequency it's also

$$g_0 \frac{k}{\omega_0} \gg 1 \,. \tag{50}$$

Therefore, the suppression factor becomes:

$$s(\omega_0) = \frac{x_0}{Z_0} = \frac{\omega_0}{k g_0} \,, \tag{51}$$

and

$$\tan \eta = \frac{1}{\tan \psi} \,. \tag{52}$$

The experimental results for $1/s(\omega)$ are reported in fig. (9) where a comparison between the data and eq.(47) are reported. The effect of the feed-back system can be appreciated

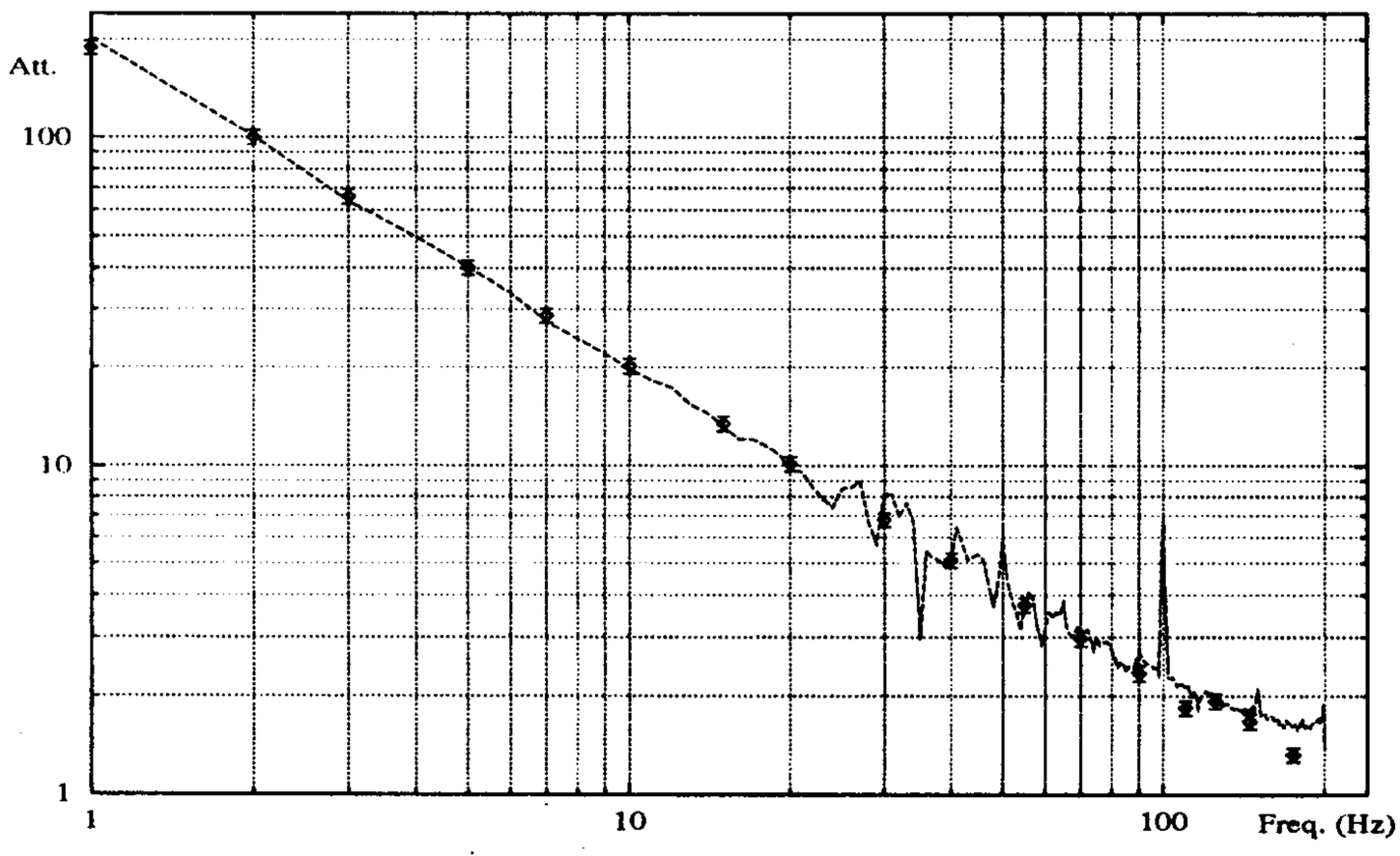

Figure 9: Attenuation factor $1/s(\nu)$.

in fig.(10) where the time behaviour of the power transmitted by the cavity is presented. The measured distribution of the power values is reported in fig.(11) and shows that the power fluctuations are always very well kept above 98% of the maximum available power. This level of stability is certainly satisfactory for our purposes.

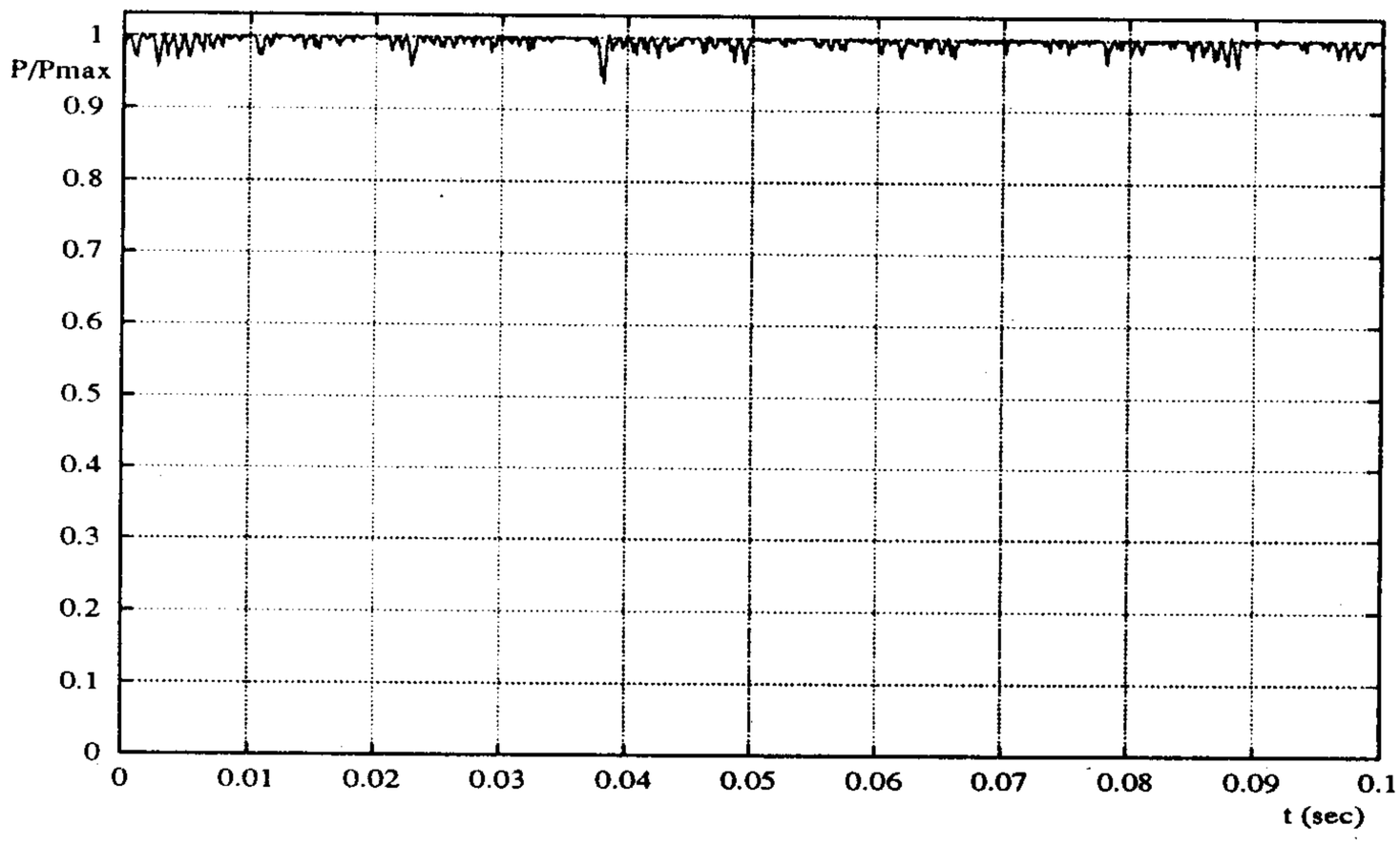

Figure 10: Transmitted power time behaviour.

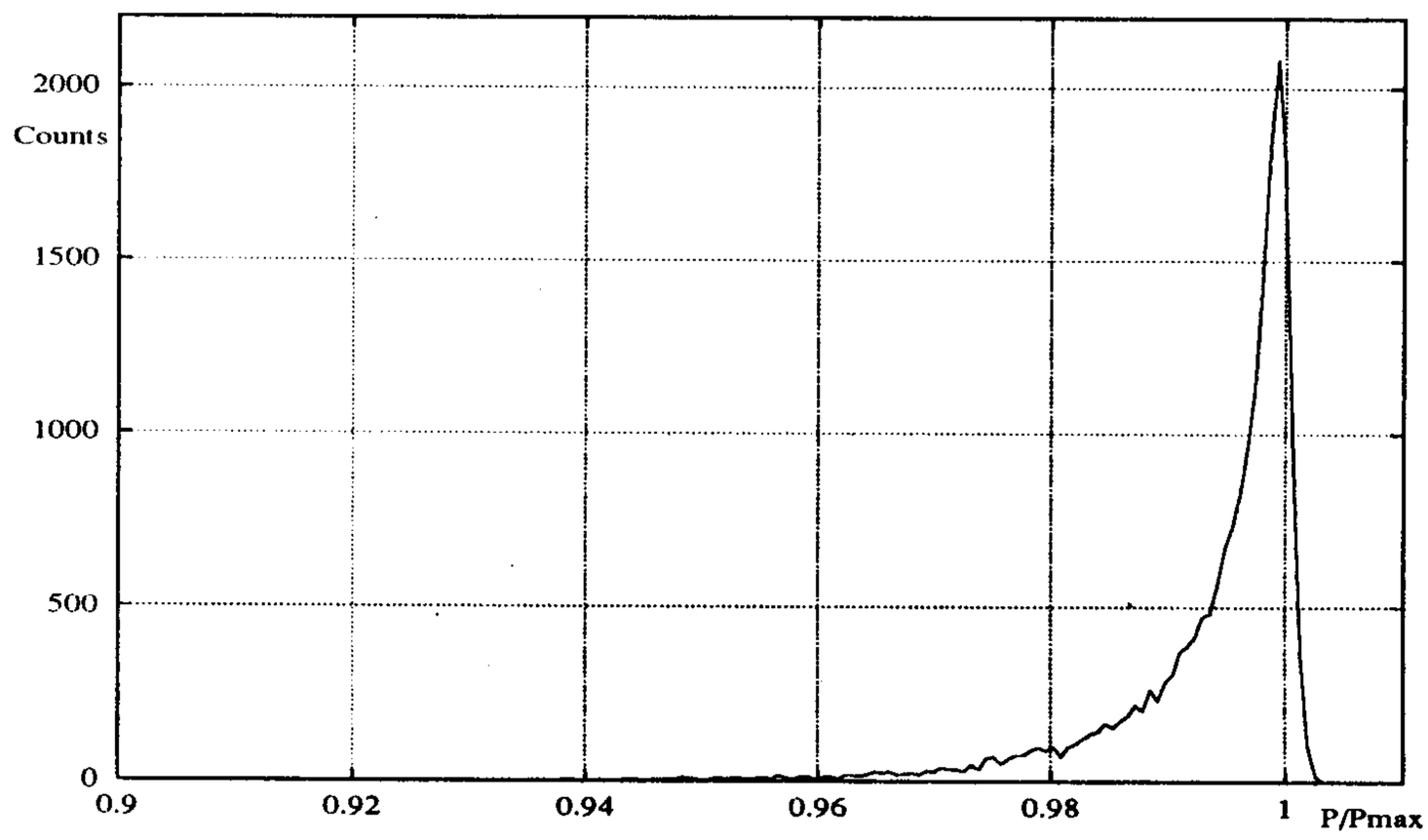

Figure 11: Transmitted power histogram.

8.4 Experimental results on the Anderson Method

Once the FP-cavity has been longitudinally locked, it is possible to start testing the automatic alignment method. According to the procedure described in sec.2, the beam transmitted through the terminal mirror of the FP-cavity hits a quadrant photodiode right in the center between two sections and the two halves of the beam generate two photocurrents. These two currents enter a tuned transformer that provides the required difference signal at the modulation frequency of 18.3 MHz. According to eq.(17), the in-phase and quadrature components of this difference provide the error signals (see fig.(12)).

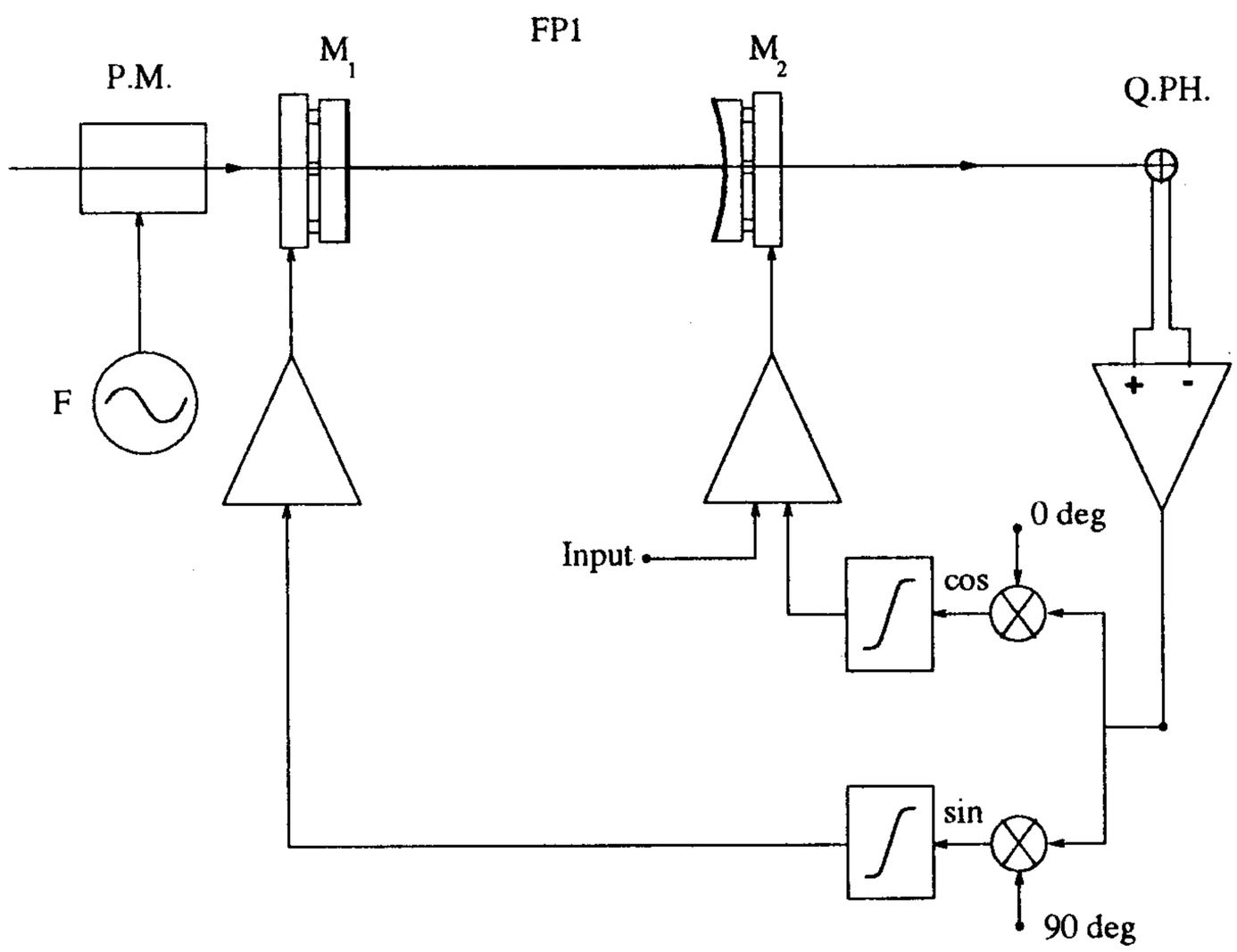

Figure 12: Feedback scheme for the angular control.

The first test of the system is to misalign the cavity and to realign it back, by turning on the feed-back loops. According to eqs.(1,2) a rotation of the terminal mirror M_2 induces a lateral off-set, while a rotation of the input mirror M_1 causes instead a displacement and a tilt: in this case both error signals are affected. Fig.(13) shows the behaviours of the two error signals, starting from a situation when both mirrors had been misaligned and the feed-back loops were turned on, one at a time.

Finally, a pink noise has been applied to M_2. The different spectra of the error signal, obtained by turning on and off the feed-back system are presented in fig.(14). The correspondent ratio (see fig.(15)) shows that the suppression factor defined by eq.(51), goes from 10 to 1 in the range $(0.5 \div 20)$ Hz.

The sensitivity limit on the angular and lateral off-set of a single Fabry-Perot, in our

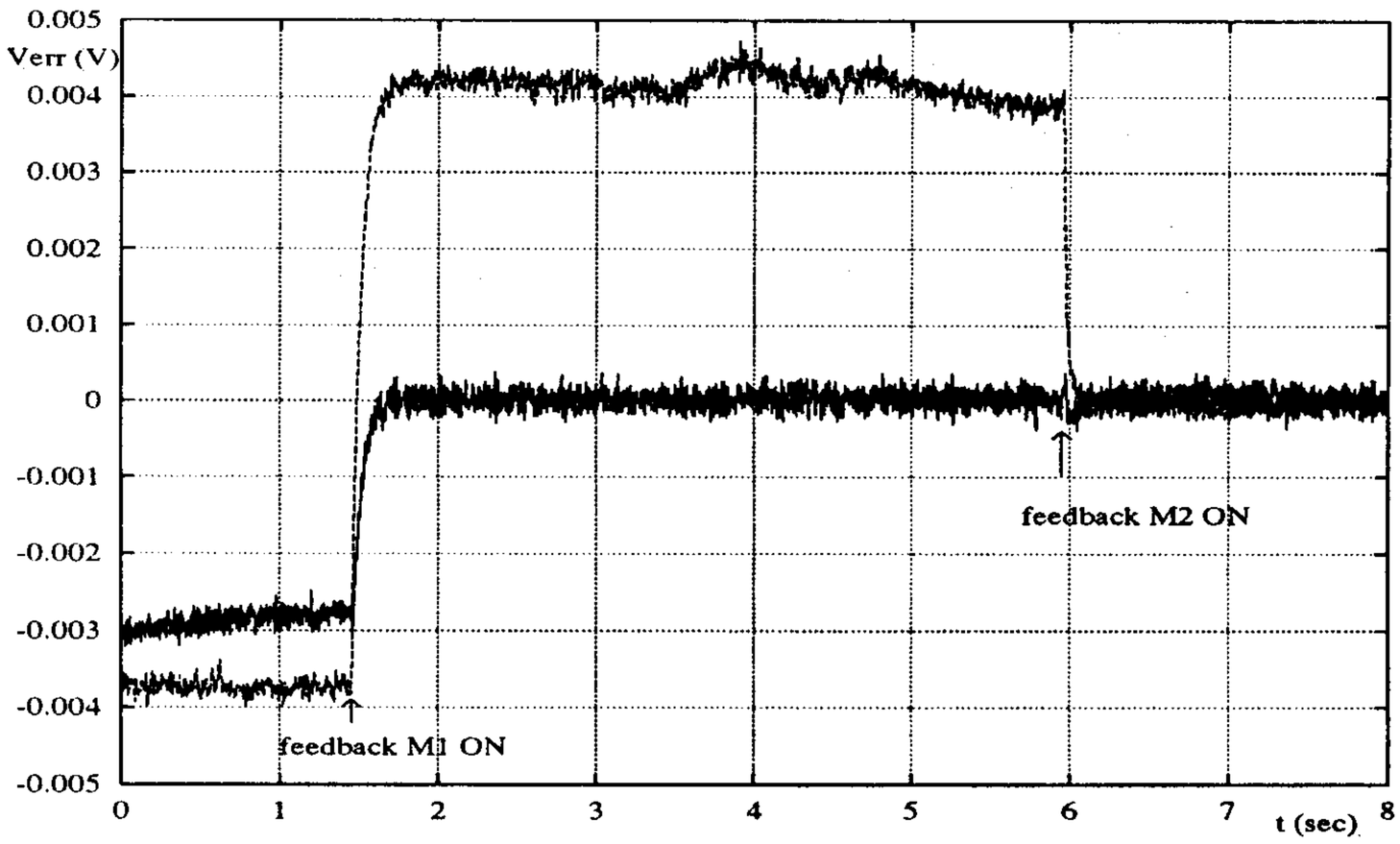

Figure 13: Time behaviour of the angular error signals.

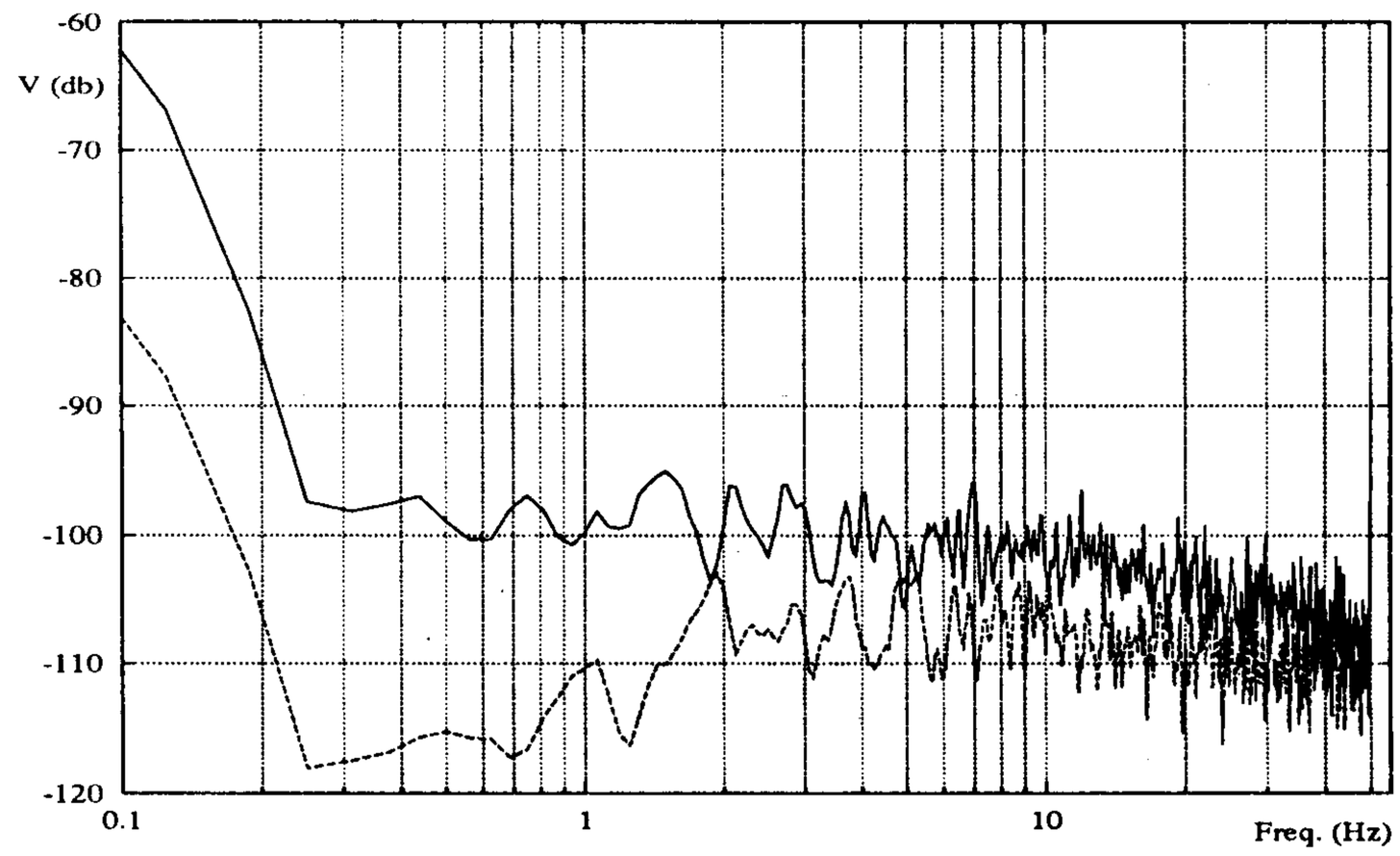

Figure 14: Spectral density of angular error signal with a pink noise.

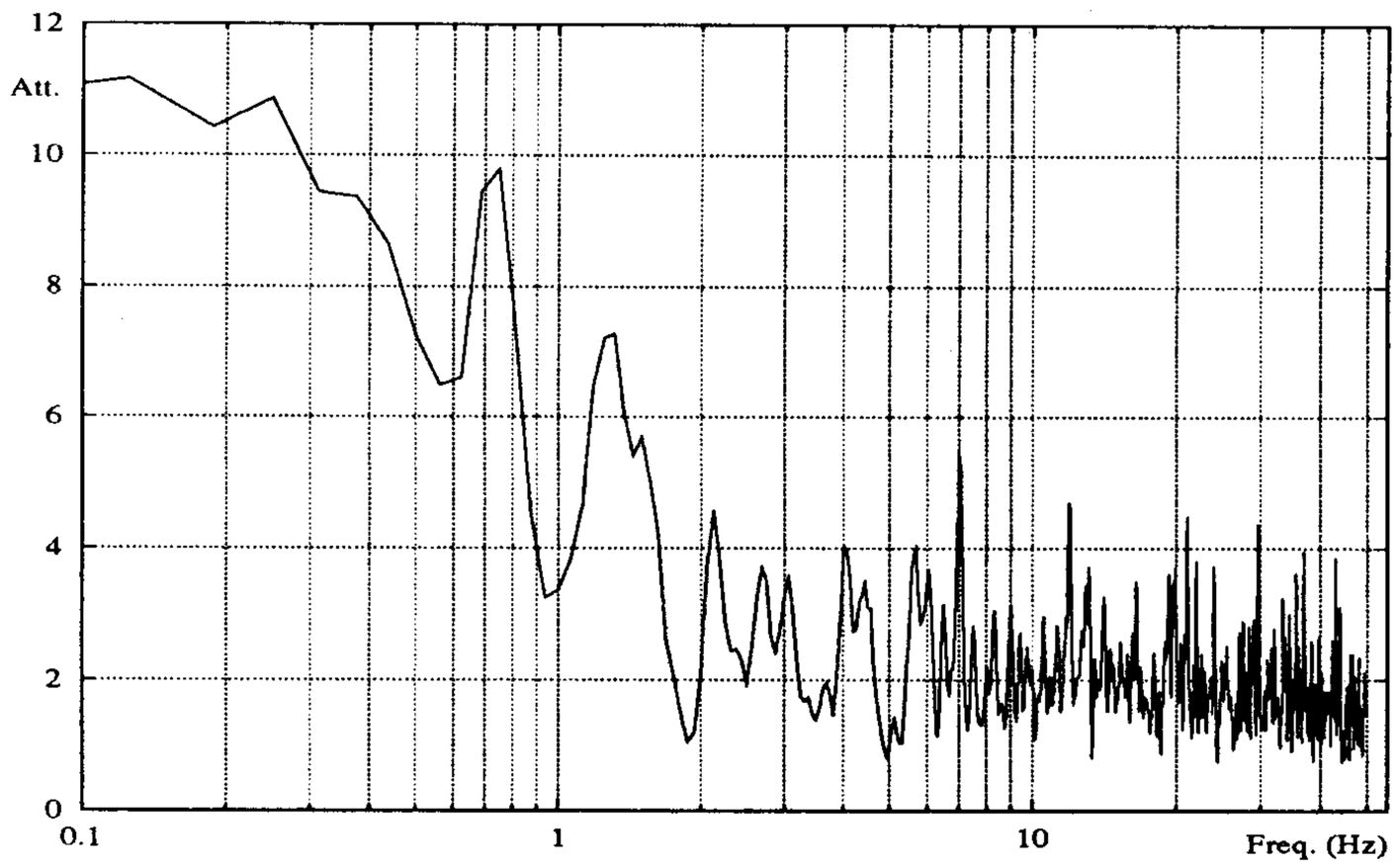

Figure 15: Suppression factor.

present experimental configuration, has been measured to be:

$$\frac{a}{w_0} = \frac{\alpha}{\alpha_0} = 4 \cdot 10^{-5} \, /\sqrt{Hz} \, . \tag{53}$$

Given the values $w_0 = 7.2 \cdot 10^{-4} \; m, \alpha_0 = 2.8 \cdot 10^{-4} \; rad$ the minimum detectable misalignments are:

$$a_{min} = 30 \; nm/\sqrt{Hz} \, , \qquad \alpha_{min} = 11 \; nrad/\sqrt{Hz} \, . \tag{54}$$

The sensitivity limit of eq.(53) expected from the shot noise is $1.2 \cdot 10^{-6} \, /\sqrt{Hz}$. Therefore, at the present stage of the experiment we are still dominated by the electronic noise.

A Basic Formulas

A.1 The S-matrix

A generic "two-ports" optical system $\mathcal{S}$ is defined as an optical assembly where two beams come in and other two beams go out (see fig.(16)).

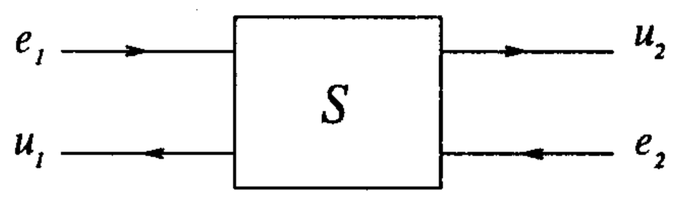

Figure 16: Generic "two-ports" optical system.

By indicating with $\mathbf{e} = (e_1, e_2)$ and $\mathbf{u} = (u_1, u_2)$ these two e.m. beam vectors, the action of the optical system is described by a (2×2) complex matrix S [7] defined by the following transformation:

$$\mathcal{S} : \mathbf{e} \rightarrow \mathbf{u} = S\mathbf{e} \, . \tag{A.1}$$

The diagonal terms S_{ii} give the fractions of the outcoming waves that result from the reflection of the incoming waves. The off-diagonal terms S_{ij} are related to the components that are transmitted by the system. By imposing the energy conservation and the invariance under time-reversal, this matrix turns out to be *symmetric* and *unitary*. This implies that its general expression depends only upon 3 independent parameters and can be written in the following form:

$$S = \begin{pmatrix} re^{i\phi_1} & -i\sqrt{1-r^2}\, e^{i\phi_+} \\ -i\sqrt{1-r^2}\, e^{i\phi_+} & re^{i\phi_2} \end{pmatrix} , \quad \det S = e^{i2\phi_+} , \tag{A.2}$$

where $\phi_+ = (\phi_1 + \phi_2)/2$.

As an example, let us consider a mirror with amplitude reflectivity r and transmittivity t related by

$$r^2 + t^2 = 1 \, .$$

Without loss of generality one can assume that the reflection causes a $90°$ *deg* phase shift [8] so that $\phi_1 = \phi_2 = \phi_+ = \pi/2$ and eqs.(A.2) become

$$S = \begin{pmatrix} ir & t \\ t & ir \end{pmatrix} , \quad \det S = -1 \, . \tag{A.3}$$

A.2 The Q-matrix

In the case of a cascade of "two-ports" optical system, it's more convenient to group the four beams of fig.(16) in a different combination of beam vectors: $\mathbf{i} = (e_1, u_1)$ and $\mathbf{o} = (u_2, e_2)$. With these definitions, the Poynting vectors associated to the corresponding components of $\mathbf{i}$ and $\mathbf{o}$ are parallel and the action of the optical system is described by a (2×2) complex matrix Q defined by the following transformation:

$$\mathcal{S} : \mathbf{i} \to \mathbf{o} = Q\mathbf{i} \,. \tag{A.4}$$

The relationship between this matrix and the S matrix defined in section A.1 is:

$$Q = \frac{1}{S_{12}} \begin{pmatrix} -\det S & S_{22} \\ -S_{11} & 1 \end{pmatrix} = \frac{\imath}{\sqrt{1-r^2}} \begin{pmatrix} -e^{\imath\phi_+} & re^{-\imath\phi_-} \\ -re^{\imath\phi_-} & e^{-\imath\phi_+} \end{pmatrix} , \tag{A.5}$$

where $\phi_- = (\phi_1 - \phi_2)/2$. This matrix is *hermitian* with

$$\det Q = \frac{1}{S_{12}^2}(-\det S + S_{11}S_{22}) = \frac{S_{21}}{S_{12}} = 1 \,. \tag{A.6}$$

In the case of the mirror considered above ($\phi_+ = \pi/2, \phi_- = 0$) one has:

$$Q = \frac{1}{t} \begin{pmatrix} 1 & \imath r \\ -\imath r & 1 \end{pmatrix} . \tag{A.7}$$

A.3 The Fabry-Perot

As shown in fig.(17), a FP-cavity can be seen as a sequence of a mirror, a drift space and a second mirror.

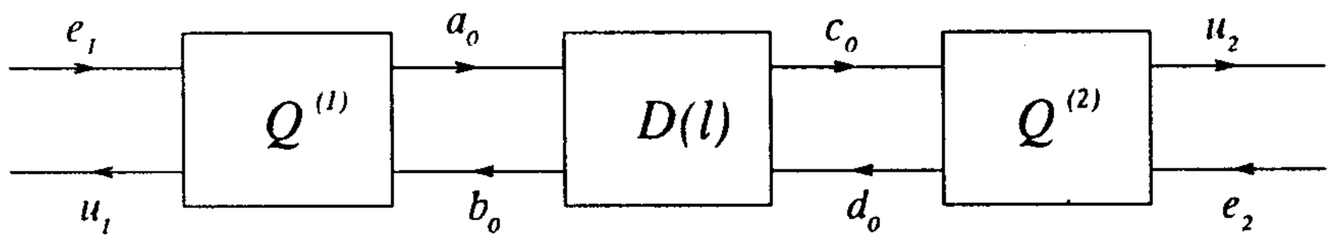

Figure 17: Q-matrices sequence for a FP.

For the two mirrors one has (see eq.(A.7)):

$$Q^{(i)} = \frac{1}{t_i} \begin{pmatrix} 1 & \imath r_i \\ -\imath r_i & 1 \end{pmatrix} , \quad r_i^2 + t_i^2 = 1 \quad (i = 1, 2) \,. \tag{A.8}$$

For a drift space of length l filled with a medium of refractive index n, the Q-matrix is:

$$D(l) = \begin{pmatrix} e^{-\imath\psi} & 0 \\ 0 & e^{\imath\psi} \end{pmatrix}, \quad \psi = \vec{k}\cdot\vec{l} = \frac{n\omega l}{c}(\hat{k}\cdot\hat{l}), \tag{A.9}$$

and can be obtained putting $r = 0$ and $\phi_+ = -\psi + \pi/2$ in the general expression (A.5). Hence, for the FP-sequence one has:

$$\Phi = Q^{(2)}D(l)Q^{(1)} = \frac{1}{t_1 t_2}\begin{pmatrix} e^{-\imath\psi} + r_1 r_2 e^{\imath\psi} & \imath r_1 e^{-\imath\psi} + \imath r_2 e^{\imath\psi} \\ -\imath r_2 e^{-\imath\psi} - \imath r_1 e^{\imath\psi} & r_1 r_2 e^{-\imath\psi} + e^{\imath\psi} \end{pmatrix}, \tag{A.10}$$

In all our considerations only the beam e_1 enters the cavity traveling along its axis and is partially reflected and transmitted. From the Q-matrix definition (A.4) and the condition $e_2 = 0$ one has

$$\begin{aligned} u_1 &= -\frac{\Phi_{21}}{\Phi_{22}}e_1 = \mathcal{R}\,e_1 = Re^{\imath\rho}\,e_1\,, \\ u_2 &= \frac{1}{\Phi_{22}}e_1 = \mathcal{T}\,e_1 = Te^{\imath\tau}\,e_1\,, \end{aligned} \tag{A.11}$$

where

$$R = \sqrt{\frac{r_1^2 + r_2^2 + 2r_1 r_2\cos 2\psi}{1 + r_1^2 r_2^2 + 2r_1 r_2\cos 2\psi}}\,, \quad \rho = \arctan\left\{\frac{r_1(1+r_2^2) + r_2(1+r_1^2)\cos 2\psi}{r_2 t_1^2 \sin 2\psi}\right\}, \tag{A.12}$$

and

$$T = \frac{t_1 t_2}{1 + r_1^2 r_2^2 + 2r_1 r_2\cos 2\psi}\,, \quad \tau = \arctan\left\{-\frac{1 - r_1 r_2}{1 + r_1 r_2}\tan\psi\right\}. \tag{A.13}$$

Depending on the value of the phase ψ, one obtains different conditions. In particular ($m \in \mathbf{N}$)

- FP on resonance[1]: $\psi = (2m+1)\pi/2$

$$\begin{aligned} R &= \frac{r_2 - r_1}{1 - r_1 r_2} & \rho &= (4m+3)\frac{\pi}{2}\,, \\ T &= \frac{t_1 t_2}{1 - r_1 r_2} & \tau &= (2m+3)\frac{\pi}{2}\,. \end{aligned} \tag{A.14}$$

[1] we are assuming $r_1 \leq r_2$

- FP off resonance : $\psi = m\pi$

$$R = \frac{r_2 + r_1}{1 + r_1 r_2} \qquad \rho = (4m+1)\frac{\pi}{2} ,$$
$$T = \frac{t_1 t_2}{1 + r_1 r_2} \qquad \tau = m\pi . \tag{A.15}$$

Finally, after some algebra, one can give the expressions for the stored beam amplitudes as well (see fig.(16)). From equations (A.10), (A.11) and fig.(17), one has:

$$a_0 = (Q_{11}^{(1)}\Phi_{22} - Q_{12}^{(1)}\Phi_{21})\, u_2 = \frac{T}{t_2} e^{i(\tau+\psi)}\, e_1 ,$$
$$b_0 = (Q_{21}^{(1)}\Phi_{22} - Q_{22}^{(1)}\Phi_{21})\, u_2 = i\frac{r_2 T}{t_2} e^{i(\tau-\psi)}\, e_1 . \tag{A.16}$$

B The Michelson Interferometer

The whole Michelson Interferometer (MI) can be seen as a sequence of optical elements in a way very similar to the one just described for the single FP-cavity. The MI-case can be conveniently discussed in the framework of a more general scheme as shown in fig.(18). As a matter of fact this scheme represents the "dual-recycling solution" and should be investigated on its own for a possible application to the Virgo case. The "single-recycling solution", which is at present adopted, is obtained as a particular case of this more general scheme.

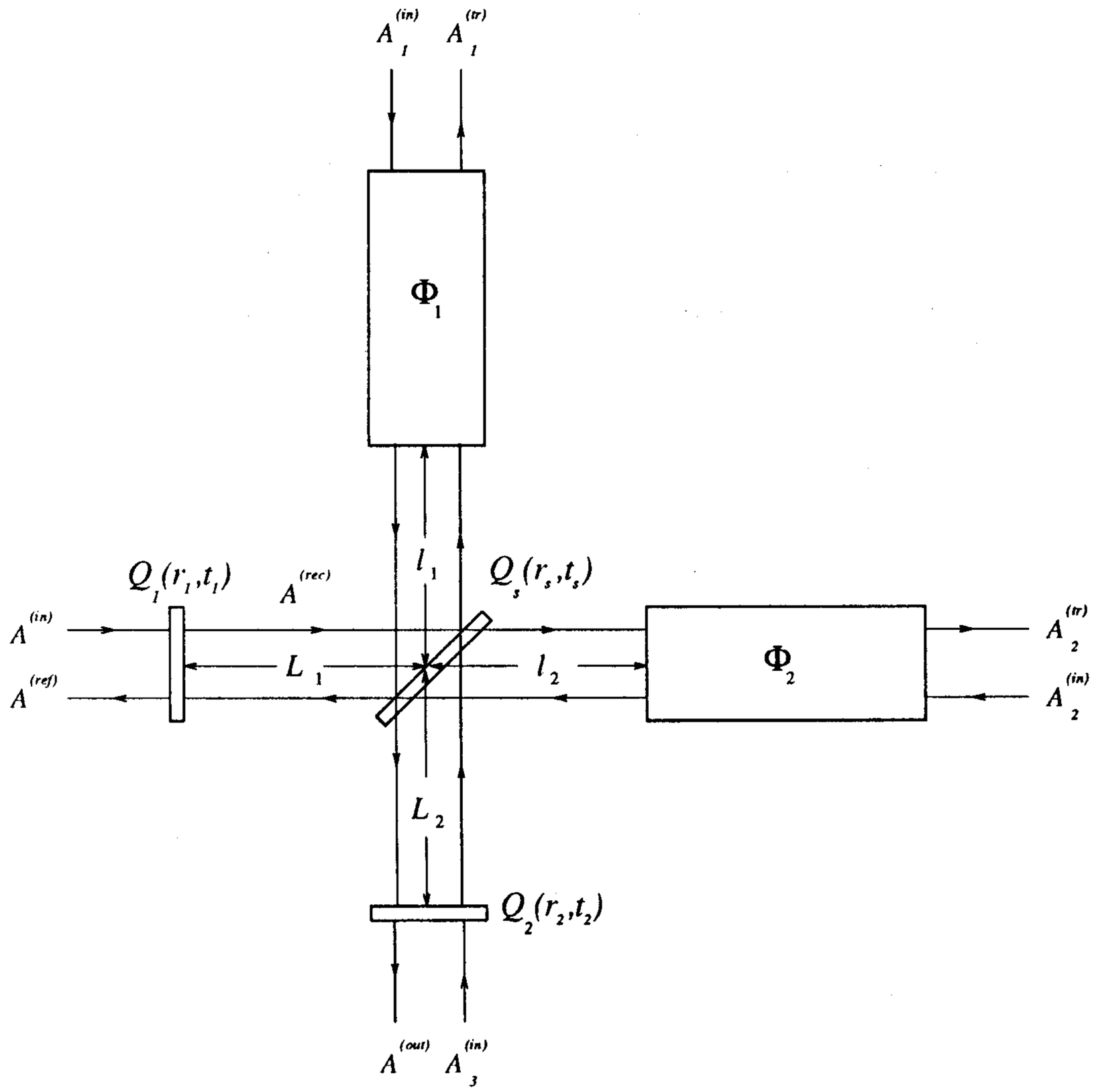

Figure 18: Michelson's interferometer scheme.

By using the same language of the previous sections, this scheme is a "four-ports" optical

system and can be pictured as shown in fig.(19).

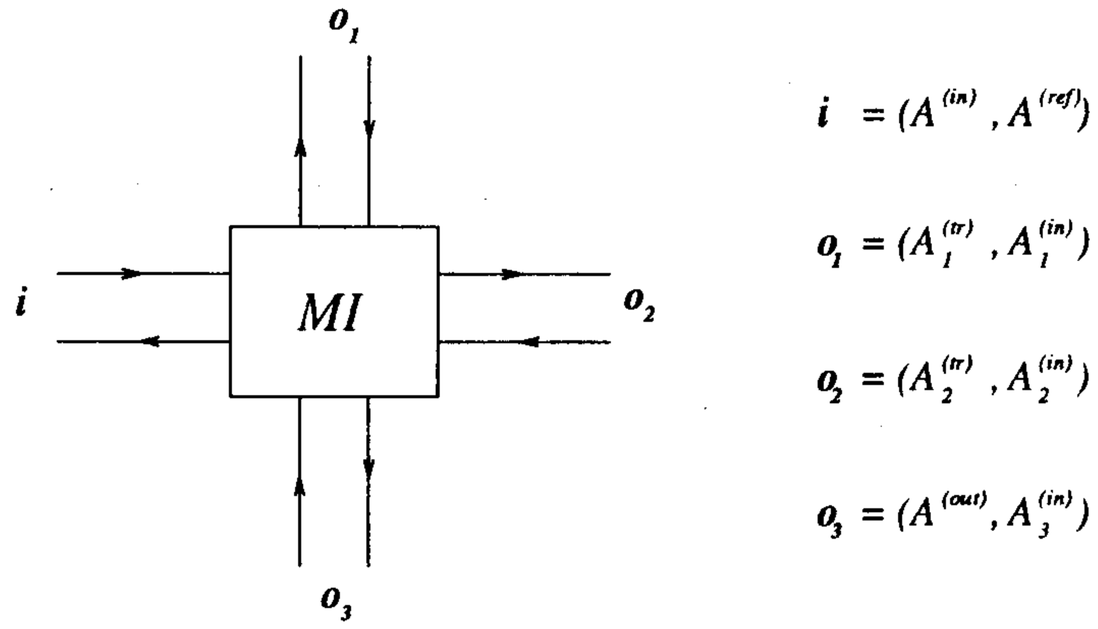

Figure 19: "four-ports" structure for MI.

Following the Q-matrix formalism, one can write:

$$\begin{aligned} \imath r_s \, \mathbf{i} &= F_3 \, \mathbf{o_1} - t_s F_2 \, \mathbf{o_3} \\ t_s \, \mathbf{i} &= F_0 \, \mathbf{o_2} - \imath r_s F_2 \, \mathbf{o_3} \end{aligned} \tag{B.1}$$

where

$$\begin{aligned} F_0 &= {Q_1}^{-1} \, D(-L_1) \, \mathbf{1} \, D(-l_2) \, {\Phi_2}^{-1} \, , \\ F_2 &= \imath \, {Q_1}^{-1} \, D(-L_1) \, \hat{\sigma}_2 \, D(-L_2) \, {Q_2}^{-1} \, , \\ F_3 &= {Q_1}^{-1} \, D(-L_1) \, \hat{\sigma}_3 D(-l_1) \, {\Phi_1}^{-1} \, , \end{aligned} \tag{B.2}$$

and

$$\hat{\sigma}_2 = \begin{pmatrix} 0 & -\imath \\ \imath & 0 \end{pmatrix} , \qquad \hat{\sigma}_3 = \begin{pmatrix} 1 & 0 \\ 0 & -1 \end{pmatrix} \tag{B.3}$$

are two Pauli-matrices, whose appearance reflects the structure of the basis vectors used to define the Q-matrix of section A.2.

In the case of no incoming beams at the output ports ($A_1^{(in)} = A_2^{(in)} = A_3^{(in)} = 0$), one can demonstrate that (see fig.(18)):

$$A^{(rec)} = t_1 \, \frac{1 - \imath r_2 C_2(t_s, r_s)}{C + \imath r_1 C_1(r_s, t_s) - \imath r_2 C_2(t_s, r_s)} \, A^{(in)} \, ,$$

$$A^{(out)} = \imath r_s t_s t_2 e^{\imath(\Gamma_1 - \Gamma_2)} \frac{C_1(1, \imath)}{1 - \imath r_2 C_2(t_s, r_s)} \, A^{(rec)} \, , \tag{B.4}$$

where

$$\begin{aligned} C &= 1 - r_1 r_2 \mathcal{R}_1 \mathcal{R}_2 e^{-\imath 2(\delta_{11} + \delta_{22})} \, , \\ C_k(x, y) &= x^2 \mathcal{R}_1 e^{-\imath 2 \delta_{1k}} - y^2 \mathcal{R}_2 e^{-\imath 2 \delta_{2k}} \, , \qquad (k = 1, 2) \end{aligned} \tag{B.5}$$

and

$$\gamma_i = \frac{\omega}{c} l_i \,, \qquad \Gamma_i = \frac{\omega}{c} L_i \,, \qquad \delta_{ij} = \gamma_i + \Gamma_j \,. \qquad (i,j = 1,2) \tag{B.6}$$

If we consider the case of single recycling ($r_2 = 0, t_2 = 1$) in the following simplifying hyphotesis:

i) 50/50 beam-splitter ($r_s^2 = t_s^2 = 1/2$)

ii) identical FP-cavities ($\mathcal{R}_1 = \mathcal{R}_2 = \mathcal{R}$)

eqs.(B.4) become:

$$A^{(rec)} = \frac{2t_1}{2 + ir_1\mathcal{R}\left(e^{-i2\delta_{11}} - e^{-i\delta_{21}}\right)} A^{(in)} \,,$$

$$A^{(out)} = \frac{i}{2} e^{i(\Gamma_1 - \Gamma_2)} \mathcal{R}\left(e^{-i2\delta_{11}} + e^{-i\delta_{21}}\right) A^{(rec)} \,. \tag{B.7}$$

B.1 Modulation

In the case of the "phase modulation" discussed in the text, the beam results from the linear combination of three amplitudes at equispaced frequencies

$$\omega_\alpha = \omega_0 + \alpha\Omega \qquad (\alpha = 0, \pm) \tag{B.8}$$

In the normal MI-operating conditions the following special requirements are simultaneously imposed to the fundamental line ($\alpha = 0$),

i) recycling cavity on resonance: $\mid A^{(rec)} \mid \ max.$

ii) dark fringe on the exit port: $\mid A^{(out)} \mid \ min.$

iii) FP-cavities on resonance: see eqs.(A.14)

These conditions are fullfilled if ($m, n \in \mathbf{N}$):

$$\delta_{11} = (2m+1)\frac{\pi}{2} \,, \qquad \delta_{21} = n\pi \,, \tag{B.9}$$

and, eqs.(B.7) become ($R_0 = R(\omega_0)$)

$$A^{(rec)}(\omega_0) = \frac{t_1}{1 - r_1 R_0} A^{(in)}(\omega_0) \,, \qquad A^{(out)}(\omega_0) = 0 \,. \tag{B.10}$$

At any specific position of the interferometer the general expression for the total amplitudes is always:

$$A_t = \sum_\alpha A(\omega_\alpha) = \sum_\alpha \mathcal{G}_\alpha A^{(in)}(\omega_\alpha) , \tag{B.11}$$

where

$$A^{(in)}(\omega_\alpha) = J_\alpha A^{(in)}(\omega_0) e^{i\alpha\Omega t} . \tag{B.12}$$

The modulation coefficients J_α satisfy to the following conditions:

$$\sum_\alpha J_\alpha^2 = 1 , \qquad J_+ = -J_- = J ,$$

and

$$\mathcal{G}_\alpha = G(\omega_\alpha)e^{i\theta(\omega_\alpha)} = \frac{2t_1}{2 + ir_1 R(\omega_\alpha) e^{i\rho(\omega_\alpha)} [e^{-i2\delta_{11}(\omega_\alpha)} - e^{-i\delta_{21}(\omega_\alpha)}]} . \tag{B.13}$$

are the coefficients that characterize the total amplitude at the given position inside the MI.

From the second of eqs.(A.12), we see that in the region around the resonance the phase of the reflected wave from a FP-cavity can be always written in the following form:

$$\rho(\omega_\alpha) = \rho(\omega_0) + \alpha\Delta\rho(\Omega) \qquad (\alpha = 0, \pm) \tag{B.14}$$

and, analogously from eq.(B.6), one can write:

$$\delta_{ij}(\omega_\alpha) = \delta_{ij}(\omega_0) + \alpha\frac{\Omega}{c}(l_i + L_j) \qquad (\alpha = 0, \pm) \tag{B.15}$$

Taking into account eqs.(A.14) and conditions (B.9), one has:

$$G(\omega_\alpha) = \frac{\sqrt{2}\, t_1}{\sqrt{2 - 2r_1 R(\omega_\alpha)(\cos\alpha\chi + \cos\alpha\xi) + r_1^2 R^2(\omega_\alpha)[1 + \cos\alpha(\chi - \xi)]}}$$

$$\theta(\omega_\alpha) = \arctan\left\{\frac{r_1 R(\omega_\alpha)(\sin\alpha\chi + \sin\alpha\xi)}{2 - r_1 R(\omega_\alpha)(\cos\alpha\chi + \cos\alpha\xi)}\right\} , \tag{B.16}$$

where

$$\xi = \Delta\rho(\Omega) - 2\frac{\Omega}{c}(l_1 + L_1) , \qquad \chi = \Delta\rho(\Omega) - 2\frac{\Omega}{c}(l_2 + L_1) \tag{B.17}$$

From the second of eqs.(B.16) we see that $\theta(\omega_0) = 0$. Furthermore, since from the first of eqs.(A.12) is $R(\omega_+) = R(\omega_-) = R$, one has:

$$\mathcal{G}_0 \in \mathbf{R} , \qquad \mathcal{G}_+ = \mathcal{G}_-^* . \tag{B.18}$$

Hence, eq.(B.13) can be written in the following form:

$$\mathcal{G}_\alpha = G_\alpha e^{i\alpha\theta} \qquad (\alpha = 0, \pm) \tag{B.19}$$

where $(G_+ = G_- = G)$

$$G = \frac{\sqrt{2}\, t_1}{\sqrt{2 - 2r_1 R\,(\cos\chi + \cos\xi) + r_1^2 R^2 [1 + \cos\,(\chi - \xi)]}}$$

$$\theta = \arctan\left\{\frac{r_1 R\,(\sin\chi + \sin\xi)}{2 - r_1 R\,(\cos\chi + \cos\xi)}\right\}. \qquad \text{(B.20)}$$

$G_0 = G(\omega_0)$, obtained from the first of these equations in the special case $\chi = \xi = 0$, coincides with the coefficient of $A^{(in)}$ in the first of eqs.(B.10). Following eq.(B.11), the total recycling amplitude is given by:

$$A_t^{(rec)} = \{\, J_0 G_0 + 2\,\imath\, JG\, \sin\,(\theta + \Omega t)\,\} A^{(in)}(\omega_0)\,, \qquad \text{(B.21)}$$

and:

$$\frac{\mid A_t^{(rec)} \mid^2}{\mid A^{(in)}(\omega_0) \mid^2} = J_0^2 G_0^2 \{(1 + g) - (g\cos 2\theta)\, \cos 2\Omega t + (g \sin 2\theta)\, \sin 2\Omega t\}\,, \qquad \text{(B.22)}$$

where

$$g = 2\left(\frac{J\,G}{J_0\,G_0}\right)^2. \qquad \text{(B.23)}$$

Following the same procedure one can obtain the expression for the total amplitude of the beam $A_t^{(out)}$:

$$A_t^{(out)} = 2\,\imath\, JH\, \sin\,(\sigma + \Omega t)\, A^{(in)}(\omega_0)\,, \qquad \text{(B.24)}$$

where:

$$H = \frac{1}{\sqrt{2}}\, R\, \sqrt{1 - \cos\,(\chi - \xi)}\; G\,,$$

$$\sigma = \theta + \arctan\left\{\frac{\sin\,(\Gamma + \chi) - \sin\,(\Gamma + \xi)}{\cos\,(\Gamma + \chi) + \cos\,(\Gamma + \xi)}\right\}, \qquad \text{(B.25)}$$

and

$$\Gamma = \frac{\Omega}{c}\,(L_1 - L_2)\,. \qquad \text{(B.26)}$$

By squaring eq.(B.24), one has:

$$\frac{\mid A_t^{(out)} \mid^2}{\mid A^{(in)}(\omega_0) \mid^2} = J_0^2 G_0^2\, h\,\{\,1 - (\cos 2\theta)\, \cos 2\Omega t + (\sin 2\theta)\, \sin 2\Omega t\,\}\,, \qquad \text{(B.27)}$$

where

$$h = \frac{1}{2} g R^2 [1 - \cos(\chi - \xi)] \qquad \text{(B.28)}$$

It's important to notice that, under the conditions expressed by eqs.(B.9), $| A^{(rec)} |^2$ and $| A^{(out)} |^2$ do not exhibit any components at the modulation frequency Ω. The frequency dependence of the 2Ω-components and the DC-level appearing in eqs.(B.22) and (B.27) are shown in figs.(20,21) for the case of an interferometer with the following optical and geometrical characteristics:

$L_1 = 255\,cm$ $\qquad$ $L_2 = 0$
$l_1 = 10\,cm$ $\qquad$ $l_2 = 15\,cm$
$l_{\mathrm{FP}_i} = 70\,cm \quad (i = 1,2)$

$t_1^2 = 8 \times 10^{-2}$ $\qquad$ $t_2^2 = 1$
FPs' in. mirr. : $t^2 = 8 \times 10^{-2}$
FPs' out. mirr. : $t^2 = 2 \times 10^{-4}$

Modulation : $J^2 = 10^{-2}$

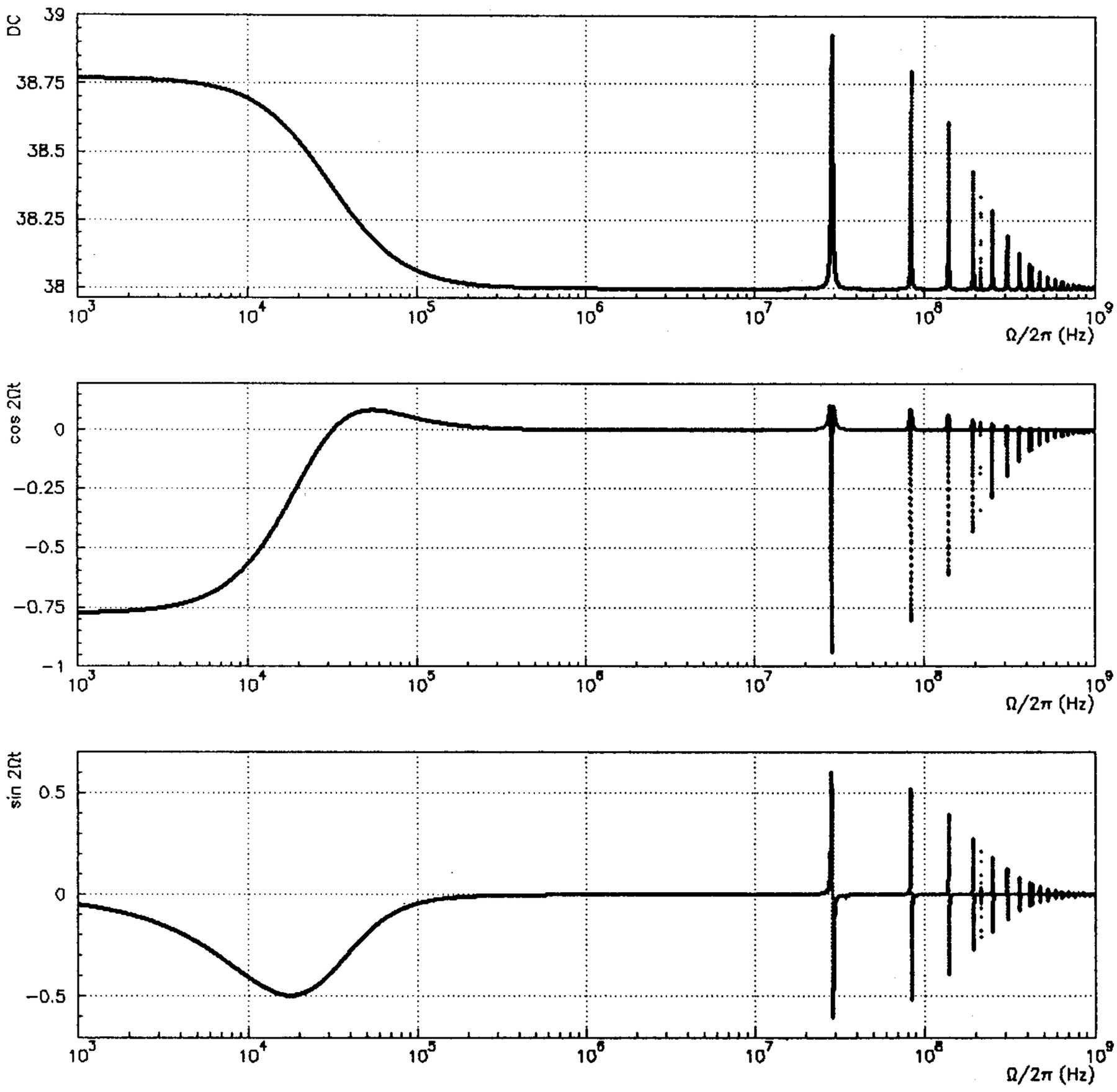

Figure 20: DC, cos $2\Omega t$, sin $2\Omega t$-coefficients in the expression of $|A^{(rec)}|^2$ (eq(B.22)).

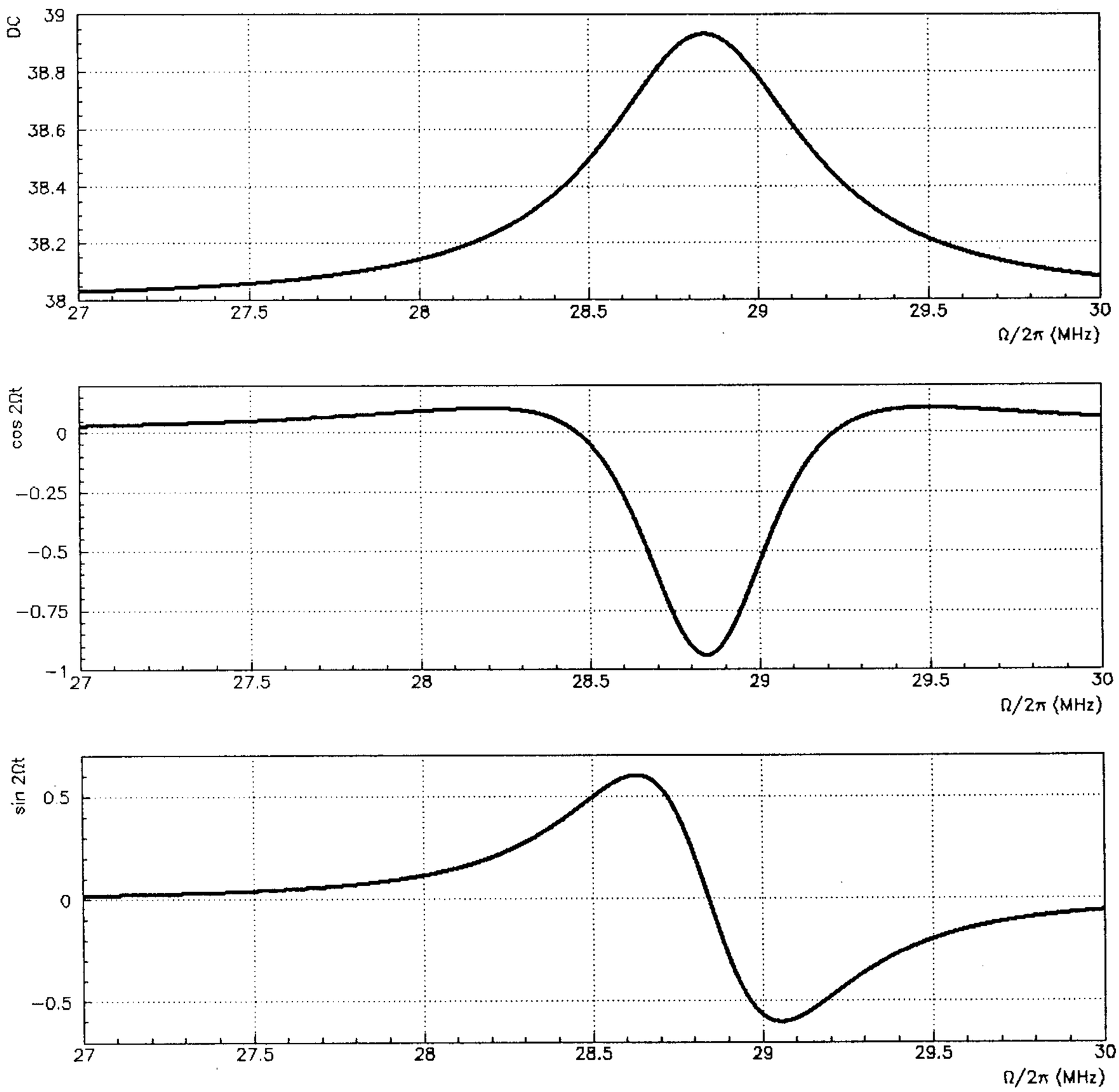

Figure 21: The same as in fig.20 in the interval $\Omega/2\pi = [27, 30]\ MHz$.

References

[1] D.Z. Anderson, *Applied Optics* 23 (1984), 2944;

[2] N.M. Sampas and D.Z. Anderson, *Applied Optics* 29 (1990), 394;

[3] E. Morrison, B.J. Meers, D.J. Robertson and H. Ward: **Experimental Demonstration of an Automatic Alignment System for Optical Interferometers,** submitted to *Applied Optics*;

[4] D. Shoemaker, P. Fritschel, J. Giaime, N. Christensen and R. Weiss, *Appl. Opt.* 30 (1991), 3133;

[5] P. Fritschel, D. Shoemaker and R. Weiss, *Applied Optics* 31 (1992), 1412;

[6] R.W.P. Drever, J.L. Hall, F.V. Kowalski, J. Hough, G.M. Ford, A.J. Munley and H. Ward, *Applied Physics* B31 (1931),97;

[7] H.A.Haus, **Waves and Fields in Optoelectronics,** Prentice-Hall (1984)

[8] M.Born and E.Wolf, **Principles of Optics,** MacMillan (1964)